ACS BIO & MED CHEM Au
AN OPEN ACCESS JOURNAL OF THE AMERICAN CHEMICAL SOCIETY

pubs.acs.org/biomedchemau
Article

Differences in the Membrane-Binding Properties of Flaviviral Nonstructural 1 (NS1) Protein: Comparative Simulations of Zika and Dengue Virus NS1 Proteins in Explicit Bilayers

Rajagopalan Muthukumaran* and Ramasubbu Sankararamakrishnan*

Cite This: ACS Bio Med Chem Au 2024, 4, 137−153
Read Online

ABSTRACT: NS1 in flaviviruses is the only nonstructural protein that is secretory and interacts with different cellular components of the host cell membrane. NS1 is localized in the ER as a dimer to facilitate viral replication. Crystal structures of NS1 homologues from zika (ZIKV) and dengue (DENV) viruses have revealed the organization of different domains in NS1 dimers. The β-roll and the connector and intertwined loop regions of wing domains of NS1 have been shown to interact with the membranes. In this study, we have performed multiple molecular dynamics (MD) simulations of ZIKV and DENV NS1 systems in apo and in POPE bilayers with different cholesterol concentrations (0, 20 and 40%). The NS1 protein was placed just above the membrane surface, and for each NS1-membrane system two to three independent simulations with 600 ns production run were performed. At the end of the production runs, ZIKV NS1 inserts deeper inside the membrane compared to the DENV counterpart. Unlike ZIKV NS1, the orientation of DENV NS1 is asymmetric in which one of the chains in the dimer interacts with the membrane while the other is more exposed to the solvent. The β-roll region in ZIKV NS1 penetrates beyond the headgroup region and interacts with the lipid acyl chains while the C-terminal region barely interacts with the headgroup. Specific residues in the intertwined region deeply penetrate inside the membrane. The role of charged and aromatic residues of ZIKV NS1 in strongly interacting with the membrane components is revealed. The presence of cholesterol affects the extent of insertion in the membrane and interaction of individual residues. Overall, membrane-binding properties of ZIKV NS1 significantly differ from its counterpart in DENV. The differences found in the binding and insertion of NS1 can be used to design drugs and novel antibodies that can be flavivirus specific.

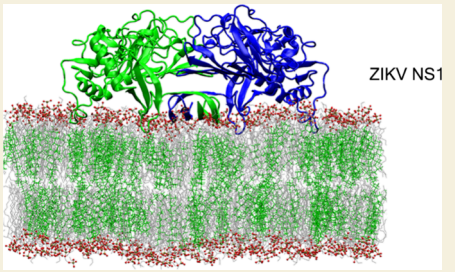

KEYWORDS: *Viral protein−membrane interactions, NS1 protein, molecular dynamics, density profile, principal component analysis*

INTRODUCTION

Flavivirus belongs to the family of *flavivridae* comprising ∼70 important human pathogens expressing high morbidity and mortality rates. Among these, the most important viruses that cause severe diseases in humans are dengue virus (DENV), West Nile virus (WNV), Japanese Encephalitis virus (JEV), and recently Zika virus (ZIKV).[1−4] Most of these flaviviral infections are vector borne, as mosquitoes primarily act as carriers to human hosts. The major risk with ZIKV is the mode of transmission since the virus has adopted to noninsect vector routes like sexual transmission, blood and platelet transfusion, as well as various body fluids, making it more vulnerable.[5,6] The primary symptom of DENV infections is a flu-like illness, which in severe cases might lead to dengue hemorrhagic fever (DHF) or dengue shock syndrome (DSS).[7] In the case of ZIKV infection, it presents as a rash, flu-like illness and rarely results in Guillain−Barre syndrome in adults, with increasing evidence for neurological abnormalities in developing fetuses.[8,9] ZIKV has gained global attention in recent years. Since its major outbreaks in 2007 and in 2016, the World Health Organization declared ZIKV as "a public health emergency of international concern". It is alarming to note that ZIKV infections have been reported in ∼66 countries including India.[10−13]

Flavivirus is an enveloped virus with (+) ssRNA and a genome size of ∼11−12 kb. The genome is made up of a single open reading frame (ORF) flanked by 5′ and 3′ untranslated regions.[14] This ORF is translated into a polyprotein, broken down to 10 structural and nonstructural proteins. The three structural proteins (C, prM and E) form the envelope and basic skeleton of the virus, while the seven nonstructural proteins (NS1, NS2A, NS2B, NS3, NS4A, NS4B, and NS5) are responsible for replication and pathogenicity.[4,15] Interestingly, among all the proteins expressed by the virus, NS1 is the only secretory protein (sNS1) and hence acts as a biomarker to identify flaviviral infection. NS1 interacts with different host cell

Received: November 20, 2023
Revised: March 1, 2024
Accepted: March 1, 2024
Published: March 15, 2024

components and aids viral growth by evading normal host cellular processes.[16] NS1 can occur in two different oligomeric states based on its function. In the dimeric state, it is localized in the ER lumen to aid in viral replication[17] and three dimers associate with lipids to form a hexameric lipoprotein to interact with the cell surface receptors.[4,18]

The mature viral NS1 is ∼350 amino acids long and exists in dimeric as well as hexameric states.[19,20] The crystal structures of DENV,[21] WNV,[21] and ZIKV[22,23] have been solved, and they all possess an overall similar structural fold. The monomeric NS1 contains three domains, namely, an N-terminal β-hairpin domain (residues 1−30), an epitope-rich wing domain (residues 31−181) and a C-terminal β-ladder domain (residues 182−352) (Figure 1a) with two potential glycosylation sites at N130

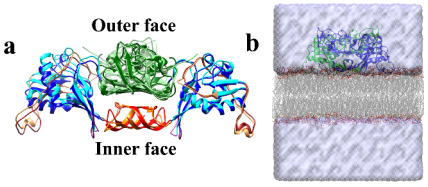

Figure 1. (a) Superposed NS1 dimer structures from Zika and Dengue viruses. The β-roll, wing, intertwined loop, and C-terminal domains of ZIKV NS1 are displayed in red, cyan, dark brown, and dark green, respectively. The same domains in DENV NS1 are shown in orange, blue, light brown, and light green, respectively. (b) Initial simulation setup of NS1-membrane complex. The two chains of NS1 are shown as cartoon representations in different colors. The membrane is shown in stick representation (gray color) and water molecules as surface representation (light gray).

and N207. There are 12 invariant cysteine residues forming six disulfide bonds per monomer and are responsible for intra-domain stabilization. The β-hairpin domain forms the dimer interface between two monomers and intertwines to form a roll-like structure called the "β-roll" dimerization domain. The wing domain can be further divided into three subdomains, namely, (i) α/β subdomain (residues 38−151), (ii) a long-intertwined loop (residues 91−130), and (iii) a discontinuous connector domain (residues 30−37 and 152−180) which connects the wing domain with the β-roll and C-terminal β-ladder domain.[21,22,24] Residue numbering followed here is according to the Zika virus NS1 protein structure with PDB ID: 5K6K.

The β-ladder domain is made up of ten β-strands, and upon dimerization, the 20 β-strands (10 from each monomer) are arranged like the rungs of a ladder (protein−protein interaction side).[24] The opposite surface of the ladder lacks a definite secondary structure and formed of loops, including spaghetti loops. Upon dimerization, NS1 has two faces: the inner face formed by the β-roll, second half of the intertwined loop, and β-ladder domain, the outer face formed by the spaghetti loop and the first half of the wing domain.[19,22,24] In the inner face, the β-roll, the connector subdomain and second half of the intertwined loop (108−130) forms a hydrophobic surface which will be favorable for the membrane interaction.[22,23] But the two flexible loops of the wing domain, the intertwined loop (residues 108−130), and the finger loop (residues 159−163) regions are not resolved in the DENV (PDB ID: 4O6B) and WNV (PDB ID: 4OIE) crystal structures.[21] However, in the recently solved ZIKV NS1 structure (PDB ID: 5K6K), these regions are visible as unstructured loops.[22] As the intertwined loop is flexible, it is speculated to be involved in the interactions either with the membrane or with other proteins.[18,23] It is reported that, after translation, a part of NS1 is localized to the ER membrane (lumen side) to help in viral replication.[17,24] Recently, an electron microscopy study on NS1 (ZIKV and DENV) explored its membrane binding property and has shown the role of NS1 in the formation of tubules protruding from the liposomal surface and inducing negative curvature which possibly hints the remodeling of ER membrane (formation of replication compartment).[25] The mutational studies have shown the loss of liposome binding activity upon substitution of residues from the finger loop (159−163), and the intertwined loop (W115, W118, and F123) in the NS1 protein.[22,24] It is also reported that NS1 interacts with the lipid rafts at the plasma membrane (which are highly enriched with cholesterol and sphingolipids). These lipid rafts are reported as preferred interaction sites for several viruses and its components.[26] Also, studies have shown that the addition of methyl-B-cyclodextrin (lipid raft inhibiting compound), lovastatin, and pravastatin (inhibitors of cholesterol synthesis enzyme HMG-CoA reductase) significantly reduces the load of NS1 secretion in DENV infection.[27] Similarly, ZIKV infection modulates the placenta lipidome for intracellular membrane reorganization (like formation of vesicle pockets on the ER luminal side visualized by TEM imaging) and viral replication.[28] Several reports have also suggested that NS1 affects cholesterol metabolism and triggers proinflammatory responses by interacting with HDL (high density lipoprotein, responsible for reverse cholesterol transport).[29−31] Recent cryo-EM studies have highlighted the formation of higher order oligomeric states (dimers and hexameric) of NS1 with HDL.[29,32] All these studies emphasize the significance of NS1 interaction with lipids and lipoproteins for replication and disease progression inside the host cells. Hence, a molecular level exploration of the interaction of NS1 with cholesterol containing membrane is necessary to understand the formation of NS1-HDL complexes.

NS1 is present in all flaviviruses and performs similar functions across the entire family. However, NS1 homologues are sequentially diverse. The two major human pathogens DENV and ZIKV share a sequence identity of ∼55% which affects the surface charge distribution, while having a similar three-dimensional structure (RMSD of 0.74 Å).[23,33] A comparative study of DENV, WNV, and ZIKV displays differences in electrostatic profiles which could have impact on the interactions of NS1 with partners like membrane, antibody, and cellular receptors.[23,34] Apart from being a potential marker for disease identification, NS1 is considered as one of the important targets in antiviral therapy. Several mutagenesis studies have explored the structure and function of NS1 domains.[35]

A few structural and computational investigations on dimeric NS1 have recently been published. Oliveira et al. used molecular dynamics simulations to study the effect of single residue substitution at position 250 (proline to leucine) that resulted in the loss of dimerization and a reduction in viral proliferation and pathogenicity in DENV NS1.[36] Similarly, Roy et al. investigated the importance of disulfide bonds in maintaining dimeric unit stability and β-ladder domain structure using extensive molecular dynamics simulations and thermodynamic analyses.[37] In addition to the structural stability of dimeric NS1, small molecule and peptide inhibitors targeting the β-roll motif domain of NS1 have been reported.[38,39]

Since ZIKV and DENV NS1 homologues share structural homology with 55% sequence identity, antibodies of ZIKV patients cross-react with those of other flavivirus including

https://doi.org/10.1021/acsbiomedchemau.3c00073
ACS Bio Med Chem Au 2024, 4, 137−153

DENV.[40−42] Computationally predicted diagnostic peptide regions in NS1 are not ZIKV specific and are not found to be common to flavivirus.[42−44] Although several studies have reported the specificity of NS1 antigens to differentiate between ZIKV and DENV, developing ZIKV antigens that can distinguish ZIKV infections from other flavivirus infections in ZIKV infected patients has remained a challenge. Although structural and inhibitory research on ZIKV and DENV has been published, the membrane binding property of NS1 is yet to be explored. Therefore, the current work employs all-atom molecular dynamics simulations to demonstrate and distinguish the membrane binding properties of NS1 (ZIKV and DENV) proteins and the possible influence of cholesterol. Our objective is to understand the role of intertwined loop in NS1 protein in binding to the membrane and to identify the crucial residues for membrane binding process. For this purpose, we used homogeneous POPE (1-palmitoyl-2-oleoyl-*sn*-glycero-3-phosphatidylethanolamine) bilayer and two different cholesterol concentrations (20% and 40%) since it is one of the major components of lipid raft. Our results show that ZIKV NS1 inserts deeper inside the membrane, interacts with different components of the membrane and has stronger affinity with the cholesterol containing bilayers than that found for DENV NS1. These studies will help to have a deeper insight into the mechanism of viral infection and the regions of NS1 proteins that can be targeted by small molecules.

METHODS

NS1 Protein Apo System Preparation and Simulation

The NS1 crystal structures with PDB ID: 5K6K (ZIKV) and 4O6B (DENV) were used as starting structures for MD simulations. The intertwined loop sections (residues 108−128) and finger loop residues (residues 159−165) are missing in the DENV crystal structure. As a result, the ZIKV crystal structure was used as a template to model these regions in DENV NS1 (ZIKV and DENV NS1 sequences share sequence identity of ∼55%). The GROMACS 5.1 software package was used to perform Molecular Dynamics (MD) simulations.[45] The structures were solvated with TIP3P water model[46] in a periodic box extended up to 12 Å from edge of the protein on all sides. The systems were neutralized by 10 and 6 Na^+ ions, respectively, for ZIKV and DENV NS1 proteins. The systems were minimized using the steepest descent and conjugate gradient approaches. The minimized structures served as initial structures for the MD simulations. The temperature of the systems was maintained at 310 K by V-rescale coupling.[47] The isothermal−isobaric ensemble was used to set the pressure to 1 bar and maintained by Parrinello−Rahman barostat.[48] The short-range electrostatic interactions were treated with a cutoff value of 12 Å. The long-range electrostatic interactions were treated with the particle-mesh Ewald method. The systems were then equilibrated for 500 ps with harmonic restrictions on protein atoms utilizing NVT and NPT ensembles. After the equilibration, the production runs of the systems in which no restraints were applied were run for a period of 600 ns each.

Preparation of NS1 Membrane Systems

The NS1 protein was manually placed over the pre-equilibrated lipid bilayer just above the lipid headgroup (distance between protein center of mass and lipid headgroup is ∼21 Å; initial structure used for MD simulation is shown in Figure 1b. Details of the preparation of pre-equilibrated lipid bilayer are provided in the Supporting Information. The overlapping lipid molecules are removed to avoid the steric clashes (∼12−15 lipid molecules were removed). The protein along with the bilayer was minimized using steepest descent and conjugate gradient methods. The system was solvated with TIP3P[46] water molecules in a periodic box with dimensions of 130 × 130 × 150 $Å^3$ ensuring at least 12 Å of water molecules between the protein and the box edge. The system was neutralized with sodium ions by replacing solvent molecules (Figure 1b) and was then equilibrated with harmonic positional restraints on the protein (backbone and side chain atoms) and lipid bilayer headgroup atoms. The restraints were gradually removed in steps of 500 ps. The temperature of the system was maintained at 310 K by V-rescale coupling.[47] The pressure was set to 1 bar using the semi-isotropic coupling scheme to a Parrinello−Rahman pressure coupling baraostat.[48] The short-range interactions were truncated with a cutoff of 12 Å. The long-range electrostatic interactions were treated with the particle-mesh Ewald method.[49] The system was equilibrated for 50 ns without restraints followed by a production run of 600 ns using the same simulation protocol described above. GROMACS modules like (rms, rmsf, density and do_dssp) were used to analyze the root mean square deviation (RMSD), root mean square fluctuation (RMSF), density plots, and secondary structures.[45] The electrostatic potentials were generated by solving Poisson−Boltzmann equation utilizing the Adaptive Poisson−Boltzmann Solver (APBS)[50,51] server and visualized using Chimera.[52] The interaction energies between NS1 and membrane were calculated by summing up the van der Waals and electrostatic energy terms with a cutoff distance of 15 Å. Principal component analysis (PCA) was performed by concatenating all the trajectories of full-length NS1 structures (1−352 residues) from all simulations. Additionally, we also performed PCA analysis by excluding the loop residues (108−130) to understand the influence of intertwined loop on NS1 dynamics. The complexes are denoted as $ZIKV_{APO}$ and $DENV_{APO}$ for NS1 without membranes, $ZIKV_{POPE}$ and $DENV_{POPE}$ for NS1 in complex with POPE neat bilayers, and $ZIKV_{CHOL20}$, $ZIKV_{CHOL40}$, $DENV_{CHOL20}$, and $DENV_{CHOL40}$ for the systems in which POPE with 20% and 40% cholesterol concentrations was used. For $ZIKV_{POPE}$, $DENV_{POPE}$, $ZIKV_{CHOL40}$, and $DENV_{CHOL40}$ complexes, three replicates were performed using the same protocol by changing the initial velocities. For $ZIKV_{CHOL20}$ and $DENV_{CHOL20}$, we performed two replicates. A total of 8 systems were simulated, and the simulation details are summarized in Table. 1. All the analyses were carried out for the replicates, and the average properties calculated for replicates are presented.

Table 1. Summary of Simulations

system	type of bilayer	system	simulation time (ns)[a]
ZIKV	NS1 apo	$ZIKV_{APO}$	600
	POPE	$ZIKV_{POPE}$	600*3
	POPE with 20% cholesterol	$ZIKV_{CHOL20}$	600*2
	POPE with 40% cholesterol	$ZIKV_{CHOL40}$	600*3
DENV	NS1 apo	$DENV_{APO}$	600
	POPE	$DENV_{POPE}$	600*3
	POPE with 20% cholesterol	$DENV_{CHOL20}$	600*2
	POPE with 40% cholesterol	$DENV_{CHOL40}$	600*3

[a]Asterisk (*) denotes number of independent replicates performed per system.

RESULTS

NS1 Sequence Variation

The flaviviral NS1 is the only viral protein that is secretory in nature and engaged in several functions, including viral reproduction, immune evasion, and pathogenesis.[35] The dimeric NS1 anchors to the ER lumen and HDL complexes for the development of the replication compartment[24,25,29,32] and triggers proinflammatory responses.[29−31] Our study aims to characterize the interactions of ZIKV and DENV NS1 proteins with the lipid bilayers and how they are affected by different membrane compositions as a function of cholesterol concen-

https://doi.org/10.1021/acsbiomedchemau.3c00073
ACS Bio Med Chem Au 2024, 4, 137−153

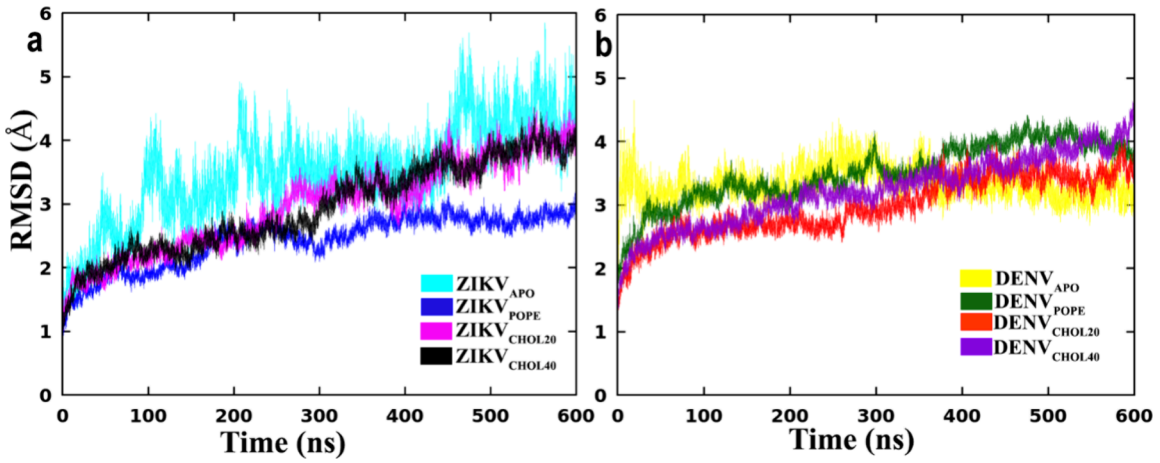

Figure 2. Time evolution of RMSD (average of replicates) of (a) ZIKV NS1 and (b) DENV NS1. RMSD calculated for the backbone atoms of NS1 dimer (both chains A and B) with respect to the starting structure. The different NS1 complexes are differentiated as $ZIKV_{APO}$ (cyan), $ZIKV_{POPE}$ (blue), $ZIKV_{CHOL20}$ (magenta), $ZIKV_{CHOL40}$ (black), $DENV_{APO}$ (yellow), $DENV_{POPE}$ (dark green), $DENV_{CHOL20}$ (red) and $DENV_{CHOL40}$ (violet). The RMSDs of POPE and 40% cholesterol complexes are the results of average of three replicates while the RMSD of 20% cholesterol complexes are due to the average of two replicates.

tration. We manually placed ZIKV and DENV NS1 above (the distance between protein center of mass and lipid headgroup is ∼21 Å) the pre-equilibrated bilayers, and two to three independent replicates of 600 ns each of all-atom molecular dynamics (three independent replicates for POPE and 40% cholesterol containing membranes and two independent replicates for 20% cholesterol containing membranes) were performed to evaluate the membrane binding properties of NS1. The results are analyzed to find out how NS1 proteins interact with the membrane and any potential differences in the mode of membrane binding and interactions between the NS1 homologues of ZIKV and DENV.

Although ZIKV and DENV NS1 homologues show sequence variation, biochemical analysis reveals that they have similar properties.[21,22] The most important property of NS1 is membrane binding and membrane remodeling for the viral replication compartment.[25,28] As the protein first encounters the lipid headgroups when binding to membranes, it is important to know the charge distribution between the two NS1 homologues. To explore this, we performed structure-based sequence alignment using ZIKV crystal structure as a reference (PDB ID: 5K6K; Figure S2). The analysis of structure-based sequence alignment reveals that frequencies of basic and aromatic residues are greater in the ZIKV NS1 homologue than that found in DENV NS1. The β-roll and wing domains (connector, intertwined loop regions) mediate contact with the lipid bilayers.[22,23,53] Hence, we focused our analysis on these domains particularly the inner face area. In the wild-type DENV NS1 protein, the residues N10, T29 of β-roll domain, Q31, Q35, Y158, T164 of connector domain, S40, A99, A141 of α/β subdomain, S103, Y113, S125, S128 of intertwined loop and N191, L206, E213, S216, T265, V286, E326, L338, N347 of C-terminal domain in DENV NS1 are substituted by basic amino acids in ZIKV NS1 (the residue numbering is with respect to ZIKV NS1 crystal structure 5K6K). Similarly, the residues N9 and E26 of the β-roll domain, Q48, S58, A77, and Q85 of the α/β subdomain, P101, Q102, P105, P112, Y122, and T129 of the intertwined loop, and A182, E192, E273, S323, and P341 of the C-terminal domain of ZIKV NS1 are replaced with basic amino acids in DENV NS1. In total, when we compared 22 positions of DENV from the β-roll and wing domain of NS1, the equivalent positions in ZIKV NS1 are occupied by basic residues. The same is true for 17 positions in ZIKV NS1 and basic residues are found in the equivalent positions in DENV NS1 (Figure S2). Also, residues T22, Q98, K122, M123, and Q175 of DENV NS1 and E178 and T256 residues of ZIKV NS1 are replaced by aromatic residues respectively in ZIKV and DENV NS1 homologues. Altogether, the inner face of ZIKV NS1 is dominated by basic residues, especially the connector domain which plays a significant role in the interaction with the membrane and to a lesser extent by aromatic residues to facilitate interaction with the lipid bilayer. We performed all-atom molecular dynamics simulations to investigate the role of basic and aromatic residues responsible for stabilizing the NS1 over a lipid bilayer at molecular level.

Conformational Dynamics of NS1 over Different Lipid Bilayers

The solvated NS1 homologues of ZIKV and DENV were initially simulated without lipid bilayers for 600 ns ($ZIKV_{APO}$, $DENV_{APO}$). The interaction of NS1 with the membrane is modeled using pre-equilibrated POPE bilayers with varying concentrations of cholesterol (0%, 20%, and 40%). Considering that the NS1 protein−lipid bilayer contact is driven by surface interaction mediated by the inner face of NS1, the protein was placed on the membrane surface and was simulated for 600 ns to allow protein insertion. The systems of NS1 investigated in neat POPE bilayers are designated as $ZIKV_{POPE}$ and $DENV_{POPE}$. The stability of NS1 was assessed by measuring the RMSDs of backbone atoms of chain A and chain B together and as individual chains (the RMSDs of the replicates were averaged for last 300 ns of the trajectory). The $ZIKV_{POPE}$ stabilized after 300 ns with minimal structural fluctuation at an average value of 2.7 ± 0.7 Å (Figure 2a). In contrast, the $DENV_{POPE}$ stabilized after 400 ns with an average value of 3.8 ± 0.4 Å suggesting overall structural stability (Figure 2b) for both the systems, although DENV NS1 exhibits higher deviation. In contrast, the cholesterol-containing systems have higher RMSDs than the NS1 systems simulated with the neat POPE bilayers. The $ZIKV_{CHOL20}$ RMSD stabilized with an average value of 3.5 ± 0.3 Å after 300 ns, whereas $DENV_{CHOL20}$ RMSD stabilized with an average value of 3.3 ± 0.3 Å after 400 ns (Figure 2b). The

https://doi.org/10.1021/acsbiomedchemau.3c00073
ACS Bio Med Chem Au 2024, 4, 137−153

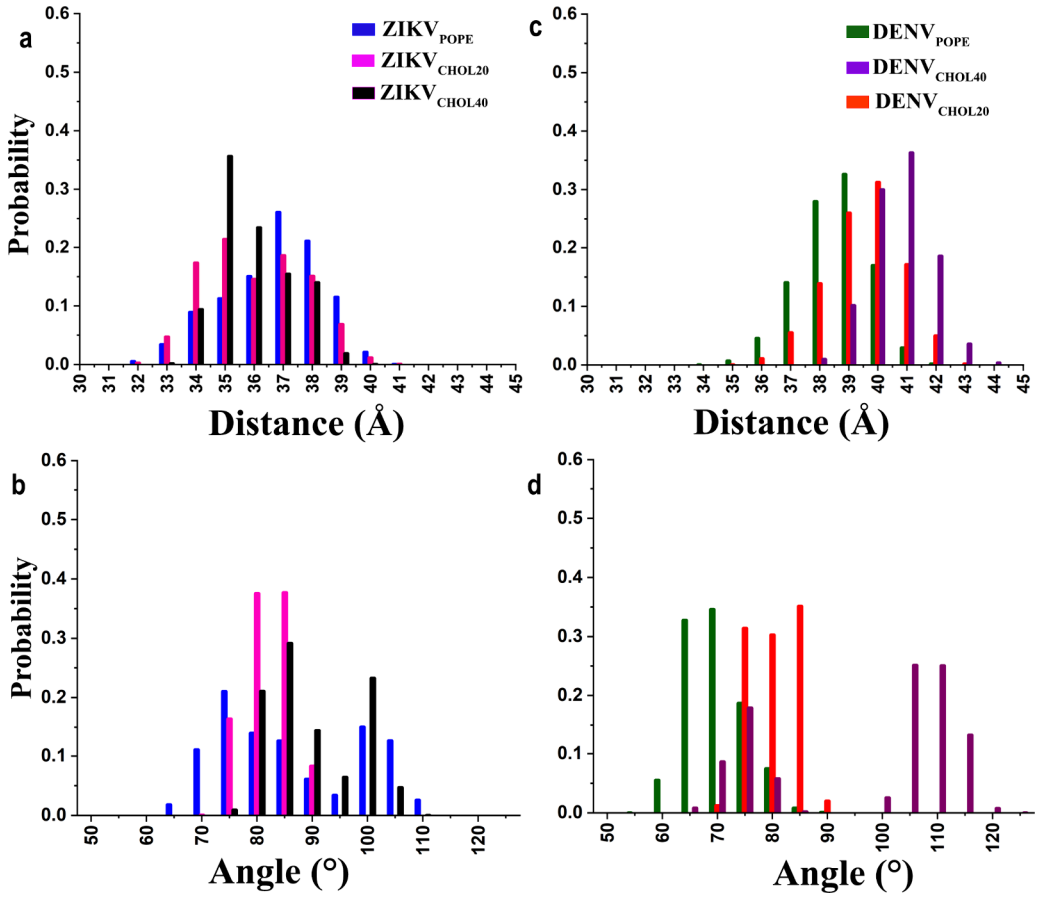

Figure 3. Histograms showing the probability distributions of (a,c) distance d and (b,d) and angle θ between membrane and NS1, and these parameters were used to characterize the orientation of NS1 with respect to the membrane for both (a, b) ZIKV and (c, d) DENV NS1 systems. The histograms are plotted by calculating the averages of these parameters from the last 300 ns of the individual replicates for each system. The NS1 complexes are differentiated as ZIKV$_{POPE}$ (blue), ZIKV$_{CHOL20}$ (magenta), ZIKV$_{CHOL40}$ (black), DENV$_{POPE}$ (dark green), DENV$_{CHOL20}$ (red) and DENV$_{CHOL40}$ (violet). The distance d of POPE and 40% cholesterol complexes are of three replicates while the distance d of 20% cholesterol complexes is of two replicates.

complexes ZIKV$_{CHOL40}$ and DENV$_{CHOL40}$ showed a more dynamic behavior as the RMSD values increased up to 4−5 Å during the initial 350 ns and shows a reduced stabilization at an average RMSD of 3.5 ± 0.5 and 3.6 ± 0.4 Å, respectively (Figure 2). In general, the presence of unstructured loops (intertwined loop and finger loop) in NS1 might have given rise to an increase in RMSD. Hence, the RMSD calculations were redone after excluding these loops. Although a similar pattern of RMSD is observed, the deletion of these unstructured loops did not show significant impact on the global RMSD for all simulated systems, affecting it by just 1 Å (Figure S3). The RMSDs of individual chains (A and B) were calculated to assess the integrity of the monomers forming the dimer (Figure S4). Table S2 shows that the RMSD for the individual chains is lower than that calculated for dimers indicating that the monomers are stable while their relative positioning might be dynamic. Such patterns of RMSD, stable monomers and relatively flexible dimer of NS1, have been observed in earlier studies also.[54−57]

In addition to the RMSD analysis, the RMSF of the Cα atoms across the 600 ns simulation period (average RMSF of triplicates) was calculated and is shown in Figure S5. Apart from a few C-terminal residues (residues 350−352 of ZIKV$_{CHOL40}$ and DENV$_{CHOL20}$) and the unstructured loop regions (residues 108−130), the RMSF exhibits stable dynamics of the overall NS1 structure (Figure S5). The previous simulations of monomeric NS1 and individual domains have shown similar flexible regions.[50,51] These flexible regions are stabilized upon dimerization. In our simulations, the intertwined loop residues (residues 108−130) of dimeric NS1 have an additional flexibility of up to 5 Å. The intertwined loop displays an unequal pattern of flexibility, with one chain exhibiting more significant fluctuation than the other (for instance, chain A of ZIKV$_{POPE}$ shows a fluctuation of ∼5 Å, whereas chain B shows ∼3 Å for residues 108−130 (Figure S5)). Notably, the hydrophobic finger loop residues (residues 155−170) exhibited higher variations in the absence of membrane (∼3.9 Å) than in membrane-bound complexes (∼3.0 Å for DENV and ∼2.0 Å for ZIKV complexes), indicating that the loop is stabilized by the membrane interactions (Figure S5).

NS1 Orientation at the Membrane

It is known that one of the crucial functions of NS1 is to interact with lipid bilayers and lipid rafts. The inner face of NS1 comprising the extended hydrophobic projections of the intertwined loop and finger loop of the wing domain is mainly responsible for this interaction.[22,23,25] Hence, we investigated the interaction of NS1 with the lipid membrane by manually placing the NS1 over the membrane such that the inner face is towards the membrane and the distance between the protein center of mass and the lipid headgroup is ∼21 Å. In general, a peripheral membrane protein can explore configurational

https://doi.org/10.1021/acsbiomedchemau.3c00073
ACS Bio Med Chem Au 2024, 4, 137−153

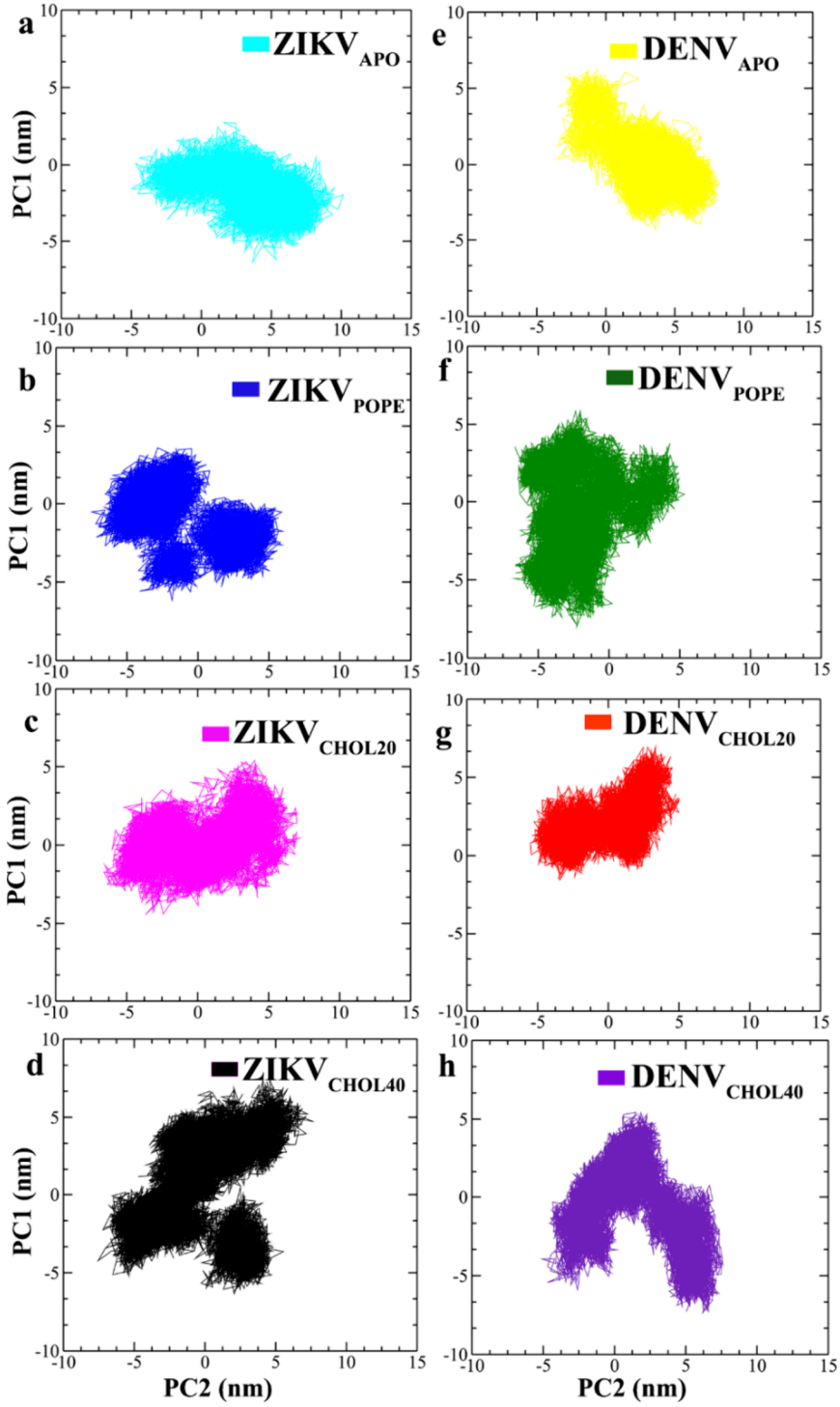

Figure 4. Principal component analysis (calculated by combining the replicates) of (a−d) ZIKV NS1, (e−h) DENV NS1. The different simulation systems are colored as follows: $ZIKV_{APO}$ (cyan), $ZIKV_{POPE}$ (blue), $ZIKV_{CHOL20}$ (magenta), $ZIKV_{CHOL40}$ (black), $DENV_{APO}$ (yellow), $DENV_{POPE}$ (dark green), $DENV_{CHOL20}$ (red), and $DENV_{CHOL40}$ (violet). The PCA plot of POPE and 40% cholesterol complexes is an average of three replicates, while the PCA plot of 20% cholesterol complexes is an average of two replicates.

dynamics by either inserting into the membrane or exploring several orientations on the surface of the membrane. Therefore, we initially explored the conformational dynamics of NS1 over the membrane by monitoring the distance and angle of inclination with respect to the membrane. The distance (d) was monitored between the center of mass of all heavy atoms of NS1 (COM_p) and the center of mass of the membrane (COM_M) (Figure S6). The angle (tilt) is calculated as the angle between the vectors linking the C-terminal residues 321−326 (β17; Figure S2) of both monomers and the membrane normal vector (Z-axis) (Figure S6). Molecular dynamics trajectories of the parameters d and θ are plotted for all the systems in Figures S7 and S8, respectively. It is clear from these trajectories that d is stabilized around 300 ns in all the systems (Figure S7). Hence, for each system, we combined the last 300 ns of the trajectories from the replicates and calculated the probability distributions of

https://doi.org/10.1021/acsbiomedchemau.3c00073
ACS Bio Med Chem Au 2024, 4, 137−153

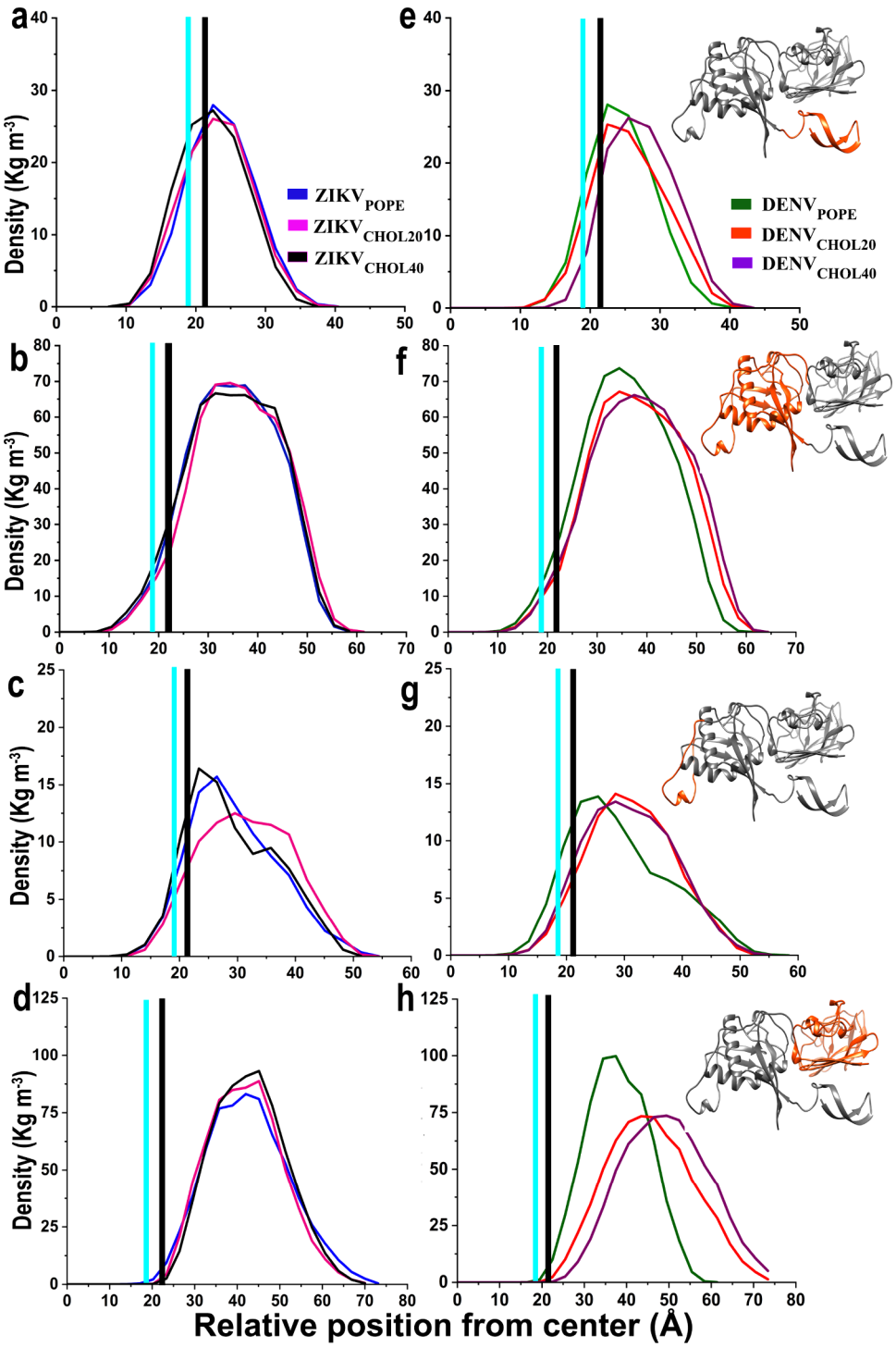

Figure 5. Average density profiles calculated for the individual domains of NS1 (chain A) along the *Z*-axis of the three different bilayers. The structure of the monomer is shown, and the respective domain used to calculate the density profiles is highlighted in orange. The different NS1 complexes are differentiated as $ZIKV_{POPE}$ (blue), $ZIKV_{CHOL20}$ (magenta), $ZIKV_{CHOL40}$ (black), $DENV_{POPE}$ (dark green), $DENV_{CHOL20}$ (red), and $DENV_{CHOL40}$ (violet). The POPE headgroup peak density position is indicated by the thick black line. The cholesterol headgroup peak density position is indicated by the cyan line. The zero on the *X*-axis corresponds to the bilayer center (as NS1 interacts with top layer and hence only top layer is shown in the figure). The profiles for individual domains are shown in rows labeled β-roll (a,e), wing (b,f), intertwined loop (c,g), and C-terminal domain (d,h) for chain A of ZIKV, DENV NS1 proteins. The density plots of POPE and 40% cholesterol complexes are an average of three replicates, while the density plots of 20% cholesterol are an average of two replicates.

distance d and the angle θ for ZIKV and DENV complexes and the histograms are shown in Figure 3.

At the beginning of the production run, the distance d remains similar for all six systems (~42.01 ± 1.1 Å, Figure S7). The reduction in the d value implies that NS1 is inserted into the membrane, whereas the increase in distance will indicate that NS1 is moving away from the membrane's center (Figure S7). This analysis shows that there is significant divergence in ZIKV

https://doi.org/10.1021/acsbiomedchemau.3c00073
ACS Bio Med Chem Au 2024, 4, 137−153

and DENV NS1 conformational dynamics. The distance d of $ZIKV_{POPE}$ varies from 33 to 39 Å with the highest probability seen at 37 Å (Figure 3). In the case of cholesterol containing systems, the distance d varies from 33 to 38 Å with the highest probability at 35 Å for $ZIKV_{CHOL20,}$ and $ZIKV_{CHOL40}$. However, in DENV systems, the distance varies from 37 to 42 Å, with the highest probability occurring at distances of 38.5, 40, and 41 Å for $DENV_{POPE}$, $DENV_{CHOL20}$, and $DENV_{CHOL40}$, respectively. Hence, it is clearly seen that ZIKV NS1 inserts deeper inside the membrane than DENV NS1 (at least 3 Å) and this difference is more pronounced in the presence of the cholesterol-containing bilayers though the initial distance d was the same for all the simulations (Figure S7). In the case of θ, the DENV NS1 system exhibits variation of $90 \pm 30^{\circ}$ while the ZIKV NS1 systems displays a much smaller variation of $90 \pm 10^{\circ}$ indicating that the angle adopted by ZIKV NS1 systems with respect to the membrane normal is close to the starting orientation.

The time evolution of the distance d reveals that ZIKV NS1 inserts deeper inside the membrane than that observed for DENV NS1, and this difference is evident irrespective of the cholesterol concentration. The insertion of ZIKV NS1 into all three membrane systems and in all the replicates is quite comparable, and there is significant overlap in the trajectories well after 350 ns with an average distance of 36.5 Å (from the center of the membrane), indicating a deeper insertion (as the starting distance is ∼42 Å). However, DENV NS1 insertion is less deep than that found for ZIKV NS1. All three DENV NS1 systems maintained the same distance until 250 ns (42 Å), however after 250 ns, $DENV_{POPE}$ and $DENV_{CHOL20}$ NS1 demonstrate a reduction in value to 39 Å, which is at least 3 Å closer to the center of the membrane (Figure S7). However, ZIKV NS1 is deeper than that of DENV NS1 by at least 3 Å as the average distance between COM_p and COM_M is 36.5 Å. In the case of $DENV_{CHOL40}$, d remains close to the initial distance of ∼42 Å (Figure S7). Although the initial distance d was the same for all six simulations, the ZIKV complexes insert deeper inside the membrane than that found for the DENV counterpart.

As the first contacts of NS1 with the membrane occur via the β-roll domain, finger loop and intertwined loop, they adopt various conformations during simulations. Hence, as mentioned earlier, the tilt angle θ was calculated using the relatively stable C-terminal domain as a reference. The MD trajectories of θ as a function of time are plotted for all six simulated systems (Figure S8). At the beginning of the production run, both ZIKV and DENV complexes ($ZIKV_{POPE}$, $DENV_{POPE}$, $ZIKV_{CHOL20}$, $DENV_{CHOL20}$, $ZIKV_{CHOL40}$, and $DENV_{CHOL40}$) remain at a θ value of 90°. However, during the simulation, the time evolution of θ shows that both the ZIKV and DENV systems tilt in comparison to the initial structure (Figure S8). The representative structures extracted from the MD trajectories of ZIKV and DENV complexes are shown in the Figures S9 and S10.

Principal component analysis helps in extracting the significant motions from the trajectory. For this purpose, we concatenated all the replicates of DENV and ZIKV, and Cα atoms were used for generating principal modes. The principal component 1 (PC1) and PC2 were extracted and projected in Figure 4. The conformational space sampled by the apo and membrane bound systems overlap but still show variations in the sampled conformational space. $DENV_{APO}$ and $ZIKV_{APO}$ systems display a single prominent cluster and sample lesser conformational space (Figure 4a, e). The $ZIKV_{POPE}$ system samples three distinct clusters, with at least two clusters partially overlapping with $ZIKV_{APO}$ in the PC1 direction (Figure 4b). $DENV_{POPE}$ (Figure 4f) relatively samples a larger conformational space than $ZIKV_{POPE}$ in the PC2 direction and exhibits partial overlap with $DENV_{APO}$. In the cholesterol containing systems, $ZIKV_{CHOL20}$ and $DENV_{CHOL20}$ sample a similar conformational space in the PC1 and PC2 directions (Figure 4c, g). The $ZIKV_{CHOL40}$ and $DENV_{CHOL40}$ complexes sample larger conformational space in the PC1 and PC2 directions (Figure 4d, h). Interestingly, $DENV_{CHOL40}$ overlaps much with the $DENV_{APO}$ in the PC1 and PC2 directions. However, $ZIKV_{CHOL40}$ overlaps to a smaller extent in the PC1 direction with $ZIKV_{APO.}$ We also investigated the role of intertwined loop in providing conformational flexibility by PCA analysis. Hence, we excluded the intertwined loop from the simulation trajectory and performed PCA analysis. It shows us that intertwined loops are assumed to be highly flexible in both systems and particularly in DENV complexes (data not shown). In general, though both ZIKV and DENV insert into membrane, PCA analysis suggests the pattern and conformational changes upon interacting with the membrane are different.

Binding of NS1 Domains to Membranes

The analysis of d and θ confirms that ZIKV and DENV NS1 interact with the membrane during simulation although the degree of insertion and the extent of interactions vary. We calculated the density distribution of the NS1 domains along with the membrane components like lipid headgroup, glycerol, and cholesterol atoms (PO4 for POPE and O for cholesterol) along the z-axis (perpendicular to the bilayer). The density distribution is plotted for chain A (Figure 5) and B (Figure S11) in which the zero on the x-axis corresponds to the lipid bilayer's center. In these figures, the black line depicts the peak density of the PO4 headgroup. The maximal densities of the lipid headgroup (PO4) of POPE, 20% and 40% cholesterol containing bilayers are 21.5, 22, and 22.9 Å, respectively. Similarly, the maximum density for cholesterol O3 atoms in these systems occurs at 19.5 Å (the cyan color line in Figure 5 for chain A and Figure S11 for chain B). When the maximum density of the NS1 domain overlaps with the density peak of the lipid PO4 group or if it is projected toward the center of the membrane, we could interpret that the domain is buried beneath the corresponding lipid group and reflects the distance from the lipid bilayer center.

The density profiles calculated for individual domains of both chains of dimeric NS1 (average values of replicates plotted) across the three distinct bilayers ($ZIKV_{POPE}$, $ZIKV_{CHOL20}$, $ZIKV_{CHOL40}$, in blue, magenta, and black colors, respectively) averaged for the replicates is shown in Figures 5 and S11. The density profile clearly helps to improve our understanding of the interaction pattern of the individual domains with different lipid components. The maximum density of the β-roll domain (∼23 Å) of both chains is close to the peak density of the phosphate headgroup and glycerol group, which enables it to interact well with the acyl groups (Figures 5a and S11a). Most of the wing domain is exposed to the solvent, and only a small portion of the wing domain, including the finger and intertwined loop, interacts with the membrane. The wing domain's maximum density (at ∼32 Å) is 10 Å away from the lipid headgroup toward the aqueous medium. Hence, it overlaps less with the headgroup density profile (Figures 5b and S11b). The uncharacterized intertwined loop (of the wing domain) extends its maximum density profile over the headgroup, and a part of the loop is well embedded into the membrane. This loop also exhibits a little

https://doi.org/10.1021/acsbiomedchemau.3c00073
ACS Bio Med Chem Au 2024, 4, 137−153

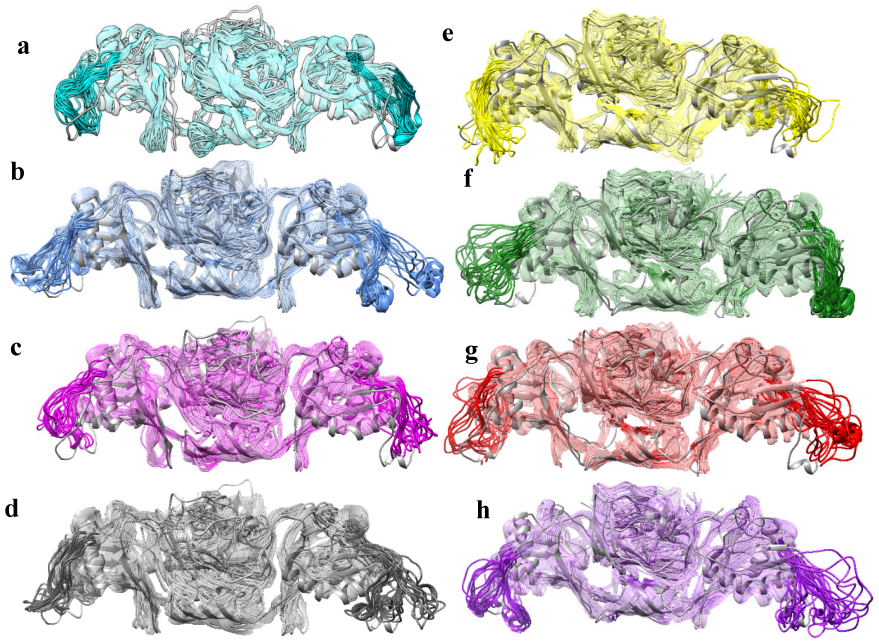

Figure 6. MD simulated NS1 structures, extracted over the last 100 ns at an interval of 20 ns for all the replicates, superposed on the initial structure (gray). The intertwined loop regions are highlighted and other regions are shown as transparent. The different simulation systems are colored as follows: (a) $ZIKV_{APO}$ (cyan), (b) $ZIKV_{POPE}$ (blue), (c) $ZIKV_{CHOL20}$ (magenta), (d) $ZIKV_{CHOL40}$ (black), (e) $DENV_{APO}$ (yellow), (f) $DENV_{POPE}$ (dark green), (g) $DENV_{CHOL20}$ (red), and (h) $DENV_{CHOL40}$ (violet). Structures are shown in ribbon representation.

insertion asymmetry between the two monomers, with chain B inserted deeper (Z = 22.4 Å) (Figure S11c) than chain A (Z = 24.5 Å) (Figure 5c). A major part of the C-terminal domain remains away from the lipid headgroup region (Figures 5d and S11d).

The NS1 density distribution of the $ZIKV_{CHOL20}$ complex (Figures 5 and S11, magenta) is analogous to that of the $ZIKV_{POPE}$ complex (shown in blue). The peak density of the β-roll domain is situated at Z = 22.4 Å, overlapping the phosphate headgroup and partly with cholesterol O3 atoms (Figures 5a and S11a, magenta). The asymmetric insertion pattern of the intertwined loop observed in $ZIKV_{POPE}$ is more prominent in $ZIKV_{CHOL20}$ as the peak densities are around Z = 27.9 Å for chain A (Figure 5c) and Z = 22.0 Å for chain B (Figure S11c). As a result, chain B intertwined loop possibly interacts better with the cholesterol atoms than chain A due to more overlap with cholesterol headgroup. The C-terminal density profile is similar to that of the $ZIKV_{POPE}$ complex (Figures 5d and S11d, blue and magenta). The $ZIKV_{CHOL40}$ system exhibits marginally more insertion than the $ZIKV_{POPE}$ and $ZIKV_{CHOL20}$ systems, as observed by the overlapping pattern of lipid headgroups. The maximal density of the β-roll domain occurs at Z = 22.5 Å (the headgroup phosphate is located at 22.9 Å); hence, it is more likely to interact with acyl chains (Figure 5a and S11a, black). Unlike $ZIKV_{POPE}$ and $ZIKV_{CHOL20}$ complexes, the intertwined loop shows a nearly symmetrical insertion profile (Z = 23.9 Å for both chains, Figure 5c and S11c, black) when ZIKV NS1 interacts with 40% cholesterol. Due to this insertion pattern, the intertwined loop can interact well with the headgroup and cholesterol molecule.

Similar to ZIKV complexes, density profiles were plotted for individual domains of DENV complexes (Figure 5e–h, chain A and Figure S11e–h, chain B). In $DENV_{POPE}$, the density profile for the β-roll domain is asymmetric (maximum density at 22.4 and 25.4 Å for chain A and chain B, respectively) (Figures 5e and S11e). Despite its overlap with the phosphate headgroup (peak density at 21.3 Å), the extent of insertion is less than that of ZIKV (~3 Å less deeply inserted). The wing domain partially overlaps with the headgroup group as much of the area is solvent exposed (Figure 5f). The intertwined loop demonstrates an uneven distribution with a maximum density at Z = 23.9 and 26.9 Å (Figures 5g and S11g), indicating that it is more solvent exposed than that found for $ZIKV_{POPE}$. Similar to $ZIKV_{POPE}$, the C-terminal domain has an asymmetric insertion pattern for two chains, and it is mostly solvent exposed (Figures 5h and S11h).

In the case of $DENV_{CHOL20}$ (red), the distribution follows a similar pattern to that of $DENV_{POPE}$ (dark green) shown in Figures 5 and S11. The maximal densities of the β-roll domain are seen at Z = 22.4 Å for chain A and 23.9 Å for chain B which overlaps with the phosphate headgroup (Figures 5e and S11e). The β-roll domain of $DENV_{CHOL20}$ is embedded deeper into the membrane than $DENV_{POPE}$ but less than $ZIKV_{CHOL20}$ (Figures 5a and S11a). Surprisingly, the intertwined loop has a symmetrical insertion distribution with a maximum density at Z = 29 Å (Figures 5g and S11g), close to $ZIKV_{CHOL20}$ (chain A, Figure 5c).

In comparison to $DENV_{POPE}$ and $DENV_{CHOL20}$, the $DENV_{CHOL40}$ has different density profiles (Figures 5 and S11, shown in violet). The maximum density of the β-roll domain is at Z = 25.4 Å for chain A (Figure 5e) and 22.4 Å for chain B (Figure S11e). The β-roll domain (chain B) overlaps with the headgroup and primarily interacts with the phosphate headgroup and occasionally with the acyl group. The intertwined loop exhibits an asymmetrical density profile with maximum density at Z = 26.9 and 25.4 Å. Hence chain B (Figure S11g) may interact more effectively with the membrane headgroup region than chain A but to a lesser extent than $ZIKV_{CHOL40}$ (Figure 5c). A significant part of the C-terminal domain remains away from the lipid headgroup region with an asymmetrical profile (Figures 5h and S11h).

https://doi.org/10.1021/acsbiomedchemau.3c00073
ACS Bio Med Chem Au 2024, 4, 137–153

Analysis of density profiles reveals the degree of insertion of domains into distinct lipid components of membranes. The β-roll domain of ZIKV complexes demonstrates relatively deeper insertion more than 3.0 Å inside the membrane than the corresponding DENV complexes. In most cases, the densities of β-roll and intertwined loop overlap with the headgroup density and partly with cholesterol, allowing the NS1 to interact with the hydrophobic regions of the lipid bilayer. The density plots and RMSF analyses (distinct fluctuations by the individual chains) reveal an asymmetric insertion profile for the intertwined loop, with one chain inserting more inside the membrane than the other. To understand this phenomenon further, we have analyzed the insertion nature of individual residues in detail.

Conformational Orientation of Spike Region at the Membrane

The intertwined loop has been implicated in membrane binding and tissue specific cell attachment in both ZIKV and DENV[18,22,23] and this is the first all-atom molecular dynamics study to evaluate interaction with a lipid membrane of variable compositions. The intertwined loop residues lack a definite secondary structure and are disordered. Due to its high flexibility, most flaviviral NS1 crystal structures failed to report intertwined structures except for the recently solved ZIKV crystal structure.[21,24,22] In this work, the intertwined loop of the ZIKV NS1 crystal structure was used as a template to model the DENV NS1 loop. During simulations, the intertwined loop region (residues 108−130) effectively inserts into the bilayer as seen through density analysis. Also, the distribution of loop density demonstrates that a part of the loop overlaps with the density of lipid membrane components, indicating that this loop region interacts with the lipid headgroup (Figures 5c, S11c and 5g, S11g). As it interacts with the membrane, it may undergo structural changes throughout simulations and adopt different conformations. We extracted the snapshots at 20 ns interval from the last 100 ns of all three independent replicates and superimposed over the initial structure (Figure 6).

We investigated MD trajectories for the presence of secondary structural changes. The time evolution of secondary structure for each amino acid in the intertwined loop (for individual replicates) was plotted using DSSP (shown in Figures S12−S14, left panel for chain A and right panel for chain B). The replicates show qualitatively similar secondary structures and hence only the consensus structure is discussed. In the apo form, residues 117−125 form β-bend, whereas the remaining regions of the intertwined loop are unstructured coil (Figure S13a, g). In the case of $ZIKV_{POPE}$, the residues 121−126 form a bend or 3_{10}-helix (at various times of simulation) in chain A (Figure S12a−c), while the same residues in chain B form a turn and 3_{10}-helix structure (Figure S12g−i). In cholesterol-containing systems, the intertwined loop often forms a β-turn or β-bend conformations as seen in the chain A and chain B (residues 113−125) of $ZIKV_{CHOL20}$ (Figure S13b, c, h, i), chain A and chain B (residues 118−128) of $ZIKV_{CHOL40}$ (Figures S14a−c, g−i).

In DENV systems, however, α-helical structures were more frequently observed. The chain A residues 118−125 $DENV_{APO}$ remain in a coil, whereas the other chain displays a beta-turn conformation (Figure S13d, j). In $DENV_{POPE}$, the chain A residues (119−126) form a helix or β-turn (Figure S12d−f) and chain B mostly remains as a coil or bend at certain regions (Figure S12j−l). In $DENV_{CHOL20}$, the chain A and B residues (119−125) forms helix or β-turn (Figure S13e, f, k, l). Similarly, the residues 118−125 in both chains adopt β-bend or β-turn conformations in $DENV_{CHOL40}$ complex (Figure S14d−f, j−l). Altogether, a β-bend or β-turn structure is common in the intertwined loops buried into the membrane, while the solvent exposed loop is present as a flexible unstructured coil.

Our analysis indicates that the intertwined loop inserts into the membrane. Hence, we measured the average insertion depth of individual residues (d_r) as an average distance between the Cα atom of each residue to COM_M in all the replicates of the simulated systems (Figures S15 and S16). For reference, the average position of the phosphate headgroup from COM_M is indicated by a yellow line, which is ∼21−22 Å from the COM_M. A d_r value of less than or close to 21−22 Å implies that the specific residue is likely to be buried beneath the phosphate headgroup. The residues of the intertwined loop are buried to varying extents in all the simulation systems.

According to the density distribution discussed earlier, an asymmetric insertion has been noted in $ZIKV_{POPE}$ and $ZIKV_{CHOL20}$ systems, while a symmetric insertion is seen in $ZIKV_{CHOL40}$ (Figures 5c and S11c, blue, magenta, and black). The d_r values of residues 117−120,122−124 of $ZIKV_{POPE}$ (chain A, B), $ZIKV_{CHOL20}$ (chain B) are below the yellow line (Figures S15a and S16a). Hence, it is inserted well into the membrane. The d_r values of $ZIKV_{CHOL20}$ (chain A) residues remains above the headgroup (yellow line) and are solvent exposed (Figure S15a). In the case of $ZIKV_{CHOL40}$, the density distribution of both chains demonstrates a symmetric insertion, and the residues 116−125 stay close (yellow line) to the phosphate headgroup level (Figures S15a and S16a). The four intertwined loop conformations (of complexes $ZIKV_{CHOL40}$, $ZIKV_{POPE}$ and $ZIKV_{CHOL20}$) which show insertion into the membrane have a common secondary structure, a β-bend or a β-turn (Figures S12−S14).

Interactions with the membrane also affect their hydration state. Hence, the number of waters within 4 Å of each of the loop residues was calculated as average of replicates and plotted in Figure S15c (chain A) and Figure S16c (chain B) for ZIKV NS1 systems. In the above analysis, residues 117−124 are prominently buried under the headgroup. Among them, the polar and charged (especially basic) residues, such as K116, K120, S121, and R125, are surrounded by higher number of water molecules than the hydrophobic residues, such as A117, G119, and V124. The general assumption of hydration state being directly proportional to insertion depth correlates only in the case of aromatic residues like W115 and W118, which are above the headgroup and well hydrated in $ZIKV_{CHOL20}$ (chain A) and $ZIKV_{CHOL40}$ (Chain B) systems (Figures S15c and S16c). The other aromatic residues Y122 and F123 are in proximity to membrane-water interface and hence remain moderately solvated in all ZIKV systems.

Similar to ZIKV systems, the average insertion profiles of the DENV NS1 (independent replicates) intertwined loop are calculated and are shown in Figures S15b and S16b. Residues 117−123 of $DENV_{POPE}$ chain A (Figure S15b) remain buried beneath the phosphate headgroup, while chain B (Figure S16b) shows less insertion except for residues A117 and W118 (staying close to the phosphate headgroup). Similarly, only residues 118−119 of $DENV_{CHOL20}$ chain A and B stay close to the headgroup and the rest of the residues are far from the phosphate headgroup (Figure S15b and S16b). The $DENV_{CHOL40}$ chain B residues 117−123 are inserted below the headgroup (below the yellow line, Figure S16b). The intertwined loops which stay close to the headgroup and

https://doi.org/10.1021/acsbiomedchemau.3c00073
ACS Bio Med Chem Au 2024, 4, 137−153

Table 2. Residues of ZIKV NS1 Having Contact with Different Lipid Groups[a]

lipid group	$ZIKV_{POPE}$	$ZIKV_{CHOL20}$	$ZIKV_{CHOL40}$
		head group	
acidic	**chain A**: E12, E26, D30, E72, E74, E81, D157, E203, E272, E309	**chain A**: D7, E12, E26, D30, E74, E80, E81, E272, E274, E278, E279	**chain A**: D1, D7, E12, E26, D30, E74, E81, D157
	chain B: E26, D30, E271, E279	**chain B**: D1, E12, D30, E74, E80, D157, E272	**chain B**: D7, E26, D30, E74, E80, E81, D157, E192, E203, E272, E274, E278, E279
basic	**chain A**: K10, R14, R29, R31, K33, R40, K69, K116, K120, H158, H164, H216, R306, R326	**chain A**: K11, R14, R29, K33, K120, R125, R214, R324, H164, H216	**chain A**: K10, K11, R14, R29, R31, K33, R40, K116, K120, R326, H158, H164, K213
	chain B: K11, R14, R29, R31, H164, R276, R306, R324, R326	**chain B**: R14, R29, R31, K33, R40, K116, R125, H158, H164	**chain B**: K10, K11, R14, R29, R31, K33, K120, H158, R214, R276, R324, H164, H216,
aromatic	**chain A**: W28, Y122, F163	**chain A**: F8, W28, Y122, F123, F160, F163	**chain A**: W28, W118, Y122, F160, F163
	chain B: W28, F163	**chain B**: W28, W118, Y122, F160, F163	**chain B**: W28, Y122, F123, F160, F163
hydrophobic	**chain A**: T13, C15, T17, V25, A27, S70, V71, G73, N82,G119, N131, G161, V162, G328	**chain A**: V6, S9, T13, C15, C16, T17, A27, S121, A126, G161, V162, P281, G282, A325, G328	**chain A**: T13, C15, C16, T17, A27, A117, G119, S121, V166, G282, G305
	chain B: T13, C15, G161, V162, T165, G328	**chain B**: T13, C15, C16, T17, A27, I66, G73, S121, V124, G161, V162	**chain B**: S9, T13, C15, C16, T17, A27, S70, S121, V124, A126, G159, G161, V162, C280, P281,G282
		acyl chain	
acidic	0	D1, D30	0
basic	**chain A**: R29	**chain A**: R29	**chain A**: R11, R29, K116, K120, H164
	chain B: R29, K120	**chain B**: R29, R125, H164	**chain B**:2 9
aromatic	**chain A**: W28, F123, W118	**chain A**: F8, Y122, F123	**chain A**: W118, Y122
	chain B: W28, F163	**chain B**: Y122, F123	**chain B**: Y122
hydrophobic	**chain A**: A117, V124,V162	**chain A**: V124	**chain A**: C15, G16,A117, G119, S121, G161, V162
	chain B: T119	**chain B**: V2, C15, V124, V162	**chain B**: C15, G161, V162

[a]The NS1−lipid contacts are classified according to the amino acid types and the lipid groups. The phosphate and glycerol backbone of lipids were together considered as headgroup, while the contacts with Acyl chains are tabulated separately. A contact is defined by a distance cutoff of 4 Å that is stable for at least 30% (90 ns) of the last 300 ns of the trajectory (calculation performed on replicates).

Table 3. Residues of DENV NS1 Having Contact with Different Lipid Groups[a]

lipid group	$DENV_{POPE}$	$DENV_{CHOL20}$	$DENV_{CHOL40}$
		head group	
acidic	**chain A**: E12, D92, D23, E127, E274, D281, D327	**chain A**: E12, D23, E274, D281, E326, D327	**chain A**: D1, E12, D23, E30
	chain B: D1, E12, E30, D157	**chain B**: E12, D23, E30, E74, E127, E274, D278, D281	**chain B**: E12, D23, E30, E74, E81, E274, D278, D281
basic	**chain A**: K9, K11, K14, K33, K116, K122, R322	**chain A**: K9, K11, K14, K33, R324	**chain A**: K9, K11, K14, H26, K33
	chain B: K14	**chain B**: K9, K11, K14, H26, K33, H77, K120, K122, K322, R324	**chain B**: K11, H26, K33, K122, K322
aromatic	**chain A**: W28, F160, F163	**chain A**: W28, F160, F163	**chain A**: W28, W118, F163, W168
	chain B: W118, F160	**chain B**: W28, W118, F160, F163	**chain B**: W8, W28, Y32, F160, F163, W168
hydrophobic	**chain A**: L13, C15, T27, T29, Q31, T117, S125, T126, G161, V162, T164, N166	**chain A**: S2, G3, C4, N10, L13, C15, C16, S17, T27, Q31, G161, V162, T164, T165, N166, G282, T300, G328, C329	**chain A**: G3, C4, N10, C15, G16, S17, T22, T27, Q31, G119, G161, T164, T165, N166
	chain B: L13, S17, G159	**chain B**: G3, C4, L13, C15, T27, T29, G119, A121, M123, L124, S125, T126, V162, T164, T165	**chain B**: L13, C15, V25, T27, T29, G119, G159, G161, T164, T165
		acyl	
acidic	0	**chain A**: D281	**chain B**: D12
basic	**chain A**: K122	**chain A**: K11, K14	**chain A**: K14
		chain B: K122	**chain B**: K14
aromatic	**chain A**: W28, W118	**chain A**: F163	**chain B**: W28, W118, F160, F163
	chain B: W118	**chain B**: W28	
hydrophobic	**chain A**:M123, L124	**chain A**: L13, C15, V162	**chain A**: S2, C15, G161, V162
	chain B: L13, T117	**chain B**: T29, G119, M123	**chain B**: L13, C15, Q31, G119, G161, V162

[a]The NS1−lipid contacts are classified according to the amino acid types and the lipid groups. The phosphate and glycerol backbone of lipids were together considered as headgroup, while the contacts with Acyl chains are tabulated separately. A contact is defined by a distance cutoff of 4 Å that are stable for at least 30% (90 ns) of the last 300 ns of the trajectory (calculation performed on replicates).

inserted into the membrane are highly probable to adopt a secondary structure (Figures S12−S14)

The DENV intertwined loop hydration profile was calculated and is shown in Figures S15d and S16d. It is observed from the secondary structure and insertion profile analysis that residues 117−123 form a secondary structure and stay closer to the headgroup than the rest of the loop residues. Similar to ZIKV systems, polar and charged (basic) residues such as K116, K120,

https://doi.org/10.1021/acsbiomedchemau.3c00073
ACS Bio Med Chem Au 2024, 4, 137−153

and S125 are more hydrated, except for T117. Residue L124 shows a nonuniform water distribution (Figures S15d and S16d). For example, in chain A of $DENV_{POPE}$, it remains below the headgroup and attracts less water (Figure S15d). In contrast, in the cholesterol containing complexes ($DENV_{CHOL20}$ and $DENV_{CHOL40}$), it attracts more water molecules due to solvent exposure (Figures S15d and S16d). The variant aromatic residues Y122 and F123 of ZIKV are substituted, respectively, by the basic and hydrophobic residues K and M in DENV NS1 at the structurally equivalent positions (Figure S2). Consequently, residue K122 is solvated by more water molecules in all three DENV complexes when inserted less (Figures S15d and S16d).

Consistent with the density plots, the ZIKV and DENV intertwined loop residues interact with the membrane, and especially residues 117−119 show uniform insertion. It is also clear that NS1 shows distinct binding dynamics with different cholesterol concentrations. Altogether, the membrane binding property influences the structure of intertwined loop residues 117−125. A possible secondary structure is observed when the loop interacts favorably with the membrane and expresses stable interactions. According to the insertion of individual residues, their hydration state is also affected.

Interface of the NS1 and Membrane Interaction

Our above analysis establishes the inner face of NS1 as the primary interacting region with the lipid bilayer. The density plot and the residue contact analyses have provided enough evidence that NS1 exhibits varying degrees of insertion in the simulated systems and that the stability of NS1-membrane interactions depends largely on the electrostatic interactions. Prior research has identified the β-roll and finger loop of the wing domain as the vital membrane-interacting regions.[22−24] Additionally, our study identifies the role of intertwined loop and the C-terminal domain in membrane binding. The lipid heavy atoms within 4 Å of each protein residue which remain in stable contact for at least 30% of the last 300 ns of all three replicate simulations are listed (in Tables 2 and 3) for both ZIKV and DENV systems.

Residues forming contacts with lipid groups (headgroup and acyl group) are classified based on the type of amino acids, such as acidic, basic, aromatic, and hydrophobic. Previous experimental, structural, and computational studies revealed the importance and preference of aromatic and basic residues in membrane-binding peptides and proteins.[58−61] All the residues forming contacts from both chains with different lipid components are listed in Tables 2 and 3. In the presence of cholesterol, the number of acidic residues forming stable contacts with the lipid headgroup in the ZIKV complexes increases for cholesterol containing systems (14 in $ZIKV_{POPE}$, 18 in $ZIKV_{CHOL20}$, and 21 in $ZIKV_{CHOL40}$). However, a very limited number of residues form contact with the acyl group (Likely due to the shorter side-chain length of acidic residues) (Table 2). The participating acidic residues of the β-roll domain (1D, 7D, E12, E25, E26, D30), wing domain (D37, D157, E74, E80, E81), and C-terminal domain (E192, E203, E272, E274, E278, E279, E309, D327) are listed in Table 2. However, no such increase in the number of residues in DENV systems is found because the insertion of DENV NS1 is not deeper inside the membrane, and the same phenomenon is observed in cholesterol-containing systems. The number of acidic residues forming contacts with the headgroup region remained between 11 and 14 in all DENV systems (Table 3). In the DENV complex, the acidic residues of the β-roll domain (D1, D23, E12, E30), wing domain (D92, D157, E37, E74, E81, E127), and C-terminal domain (E274, E276, E326, D278, D281, D327) are involved in the interactions with lipid head groups.

In addition to acidic residues, the interaction formed by basic residues with distinct lipid groups in ZIKV and DENV are listed (Tables 2 and 3). The number of residues forming interactions in ZIKV NS1 is significantly larger than that found in the DENV complex. In the $ZIKV_{POPE}$, $ZIKV_{CHOL20}$, and $ZIKV_{CHOL40}$ complexes, 23, 19, and 26 residues form stable contacts with the headgroup. There were only 8, 15, and 10 basic residues in the $DENV_{POPE}$, $DENV_{CHOL20}$, and $DENV_{CHOL40}$ complexes that are in close contacts with the lipid components. The basic residues in the β-roll (K10, K11, R14, and R29), wing (K33, R31, H35, R40, K116, K120, R125, H164), and C-terminal (K326, R214, H216, R276, R306, and R324) domains of ZIKV NS1 contribute to the interactions with the lipid headgroup (Table 2). A slight increase in the number of residues forming contacts in the $ZIKV_{CHOL40}$ complex is observed compared to those found for $ZIKV_{POPE}$. Also, the longer side chains of basic amino acids facilitate interaction with acyl groups of the bilayer. Similar to interaction with the headgroup, the basic residues of ZIKV forms higher contacts with acyl groups than DENV basic residues (Tables 2 and 3). The main interacting basic residues of DENV NS1 proteins are from β-roll (K9, K11, K14, H26), wing (H77, K116, K120, K122), and C-terminal (K272, R299, R322, R324) domains. However, a steady rise in the number of interactions in the presence of cholesterol was not seen, as the number of contacts formed by $DENV_{CHOL40}$ is lesser than that found for $DENV_{CHOL20}$ (Table 3). Our density analysis also showed that $DENV_{CHOL40}$ is less inserted than $DENV_{POPE}$ and $DENV_{CHOL20}$ systems. It is clear that the higher number of basic residues found in ZIKV (K10, R29, R31, H35, R40, R125, H164, R276) in the lipid-contacting regions compared to the same regions in DENV are due to deeper insertion of ZIKV NS1 inside the membrane. These differences in contacts and insertion between ZIKV and DENV will also reflect in their interaction energies with the membrane. Hence, we calculated the interaction energy between NS1 and membrane by summing up the van der Waals and electrostatic energy terms with a cutoff distance of 15 Å (see Appendix 2 in the Supporting Information; Table S3). The interaction energy is dominated by electrostatic energy especially in the ZIKV complexes, reflecting the role of charged residues. Also, we calculated the electrostatic potential of the inner face to understand the distribution of these charged residues (Figure S17).

The aromatic residues forming contact with lipid groups in different simulated systems are listed in Tables 2 and 3. Notably, the number of aromatic residues interacting with the headgroup did not differ significantly between the ZIKV and DENV systems. Nevertheless, in the cholesterol systems, the longer aromatic side chains form a considerable number of interactions with the acyl chain groups in ZIKV (5, 6, and 3) than in DENV (3, 2, and 4). The inner surface of NS1 has several hydrophobic residues, particularly in the β-roll domain, finger loop, and intertwined loop regions. Consequently, the number of hydrphobic residues involved in the contact is considerably larger than the basic and acidic residues (Tables 2 and 3). These residues interact significantly with the acyl chain groups of the bilayer due to their longer side chains. Interestingly, in $DENV_{CHOL20}$ NS1 more hydrophobic residues are involved in contact with the lipid headgroup than that of ZIKV NS1 hydrophobic residues (Table 3). Perhaps, the hydrophobic part of the side chain of basic residues replaced these hydrophobic

https://doi.org/10.1021/acsbiomedchemau.3c00073
ACS Bio Med Chem Au 2024, 4, 137−153

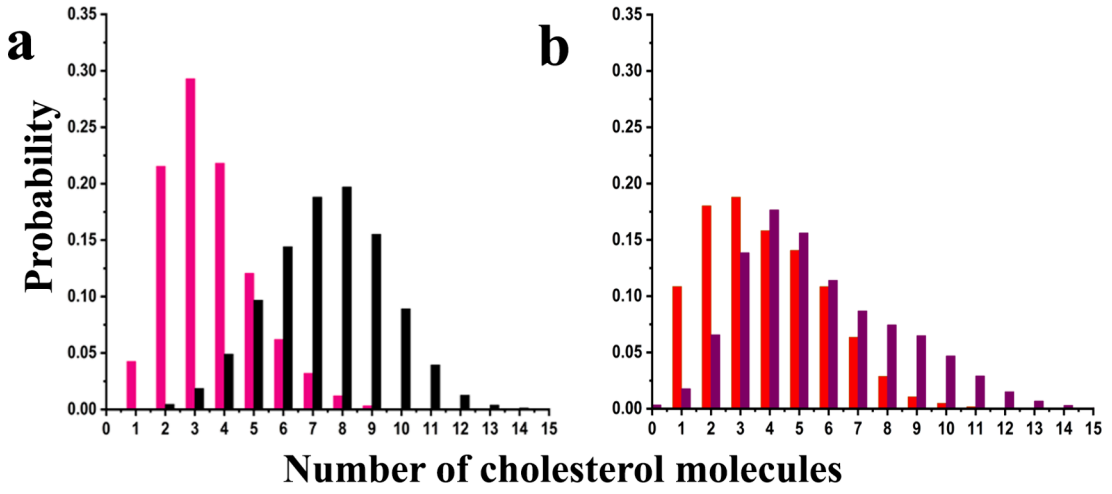

Figure 7. Distribution of cholesterol molecules within 4 Å of any residue (average values calculated for replicates) in ZIKV (a) and DENV (b) NS1 plotted as a probability. The different simulation systems are depicted as follows: $ZIKV_{CHOL20}$ (magenta), $ZIKV_{CHOL40}$ (black), $DENV_{CHOL20}$ (red), and $DENV_{CHOL40}$ (violet). The number of cholesterol molecules of 40% cholesterol complexes is an average of three replicates while the numbers of cholesterol molecules of 20% cholesterol complexes are an average of two replicates.

contacts. Overall, the contact analysis gives an idea about the interaction of NS1 with the hydrophobic part (acyl group) of the membrane. Hence, it is expected for NS1 to form interactions with cholesterol groups present in the hydrophobic part of the bilayer. Also, studies have shown that NS1 interacts with lipid rafts enriched with cholesterol.[24,26]

Thus, we have included cholesterol in our studies to explore the binding of NS1. The affinity of NS1 toward cholesterol was monitored by calculating the number of cholesterol molecules within 4 Å of NS1. Figure 7 shows the probability distribution of cholesterol around NS1. Not surprisingly, the increased distribution (ranging from 4 to 11) in $ZIKV_{CHOL40}$ indicates that the number of interacting cholesterol molecules is greater in the 40% cholesterol complex as compared to 20% cholesterol complex.

Around NS1 in $ZIKV_{CHOL20}$, a maximum of 3 to 4 cholesterol molecules are seen. However, 7 to 8 cholesterol molecules are found around $ZIKV_{CHOL40}$ NS1 protein (Figure 7a). The $DENV_{CHOL20}$ complex has 3 to 4 cholesterol molecules (corresponding to the $ZIKV_{CHOL20}$ complex), but the $DENV_{CHOL40}$ system contains 4 to 5 cholesterol molecules (Figure 7b). If we assume the rise in cholesterol around the $ZIKV_{CHOL40}$ is due to an increase in the total amount of cholesterol molecules in the system, we should expect a similar impact for $DENV_{CHOL40}$, which is not the case. Therefore, the rise in the number of cholesterol molecules in $ZIKV_{CHOL40}$ may be the result of higher number of contacts with NS1 and also due to deeper insertion inside the membrane. The analysis reveals both $ZIKV_{CHOL20}$ and $DENV_{CHOL20}$ NS1 proteins prefer to interact with cholesterol but at 40% cholesterol concentration $ZIKV_{CHOL40}$ alone shows higher interactions.

Altogether, the ZIKV complexes interact more with the bilayer than DENV complexes. Previous experimental studies have reported the role of several residues of the β-roll domain (F8, R10, and, W28), the conserved intertwined loop residues (W115 and W118) along with other residues (Y122, F123, and V123 in ZIKV; K122, M123, and L124 in DENV) to mediate membrane interactions which corroborate well with our simulations also.[22−24] Additionally, our study identifies the residues of the intertwined loop of ZIKV (K116, A117, G119, S121, V124, K120, and R125) and DENV (K116, K122, A117, G119, L124, S125, T126) to involve in stable contacts with the lipid membrane. A previous mutagenesis experiment on the greasy finger loop residues (residues 159−162) has revealed an important role for the finger loop region in membrane binding, which also agrees well with our study.[21] The membrane interacting residues identified in our study overlap well with the inhibitor-binding site residues reported through molecular docking and virtual screening studies[38,39]

DISCUSSION

Flaviviruses are responsible for human infections that cause illnesses with high rates of morbidity and death. NS1 is a flavivirus nonstructural protein that has a variety of roles in viral replication and pathogenesis. Among the multiple roles of flaviviral NS1, membrane binding is critical for viral replication since it triggers the formation of a replication compartment. As cholesterol metabolism is modulated by the flaviviruses, one of our main objectives is to understand the influence of cholesterol over the membrane bound NS1 and investigate the sequence variation of DENV and ZIKV in their membrane binding property using all-atom molecular dynamics simulations.

The study reveals that both DENV and ZIKV NS1 interact with membrane through the β-roll, partly the wing domain, and the C-terminal domain. ZIKV NS1 expresses more affinity for membrane binding than DENV. Previous mutational studies along with TEER (transepithelial/transendothelial electrical resistance) assay have revealed the critical role of intertwined loop residues 101−135 in the differential binding of NS1 with different cell lines, and the role of W115-X-X-W118-G119 (WXXWG) motif to induce endothelial hyperpermeability in HPMEC and initial cell attachment.[18] Accordingly, our study shows that the intertwined loop residues 117−124 of ZIKV and DENV prominently interact with the membrane. In the presence of cholesterol, ZIKV NS1 interacts more favorably when compared to DENV complexes. In particular, the residues 117, 118, and 119 of the WXXWG motif are buried below the level of the headgroup. A similar insertion profile for the WXXWG motif was shown previously by coarse-grained simulations of the ZIKV African and Brazilian strains.[56] The insertion profile reinforces the role of the intertwined loop and WXXWG motif in anchoring the NS1 to the cell surface and

https://doi.org/10.1021/acsbiomedchemau.3c00073
ACS Bio Med Chem Au 2024, 4, 137−153

membrane. This characteristic interaction pattern of ZIKV NS1 toward cholesterol containing membranes might be responsible for the tissue specific interaction of flavivirus for invoking endothelial hyperpermeability.

NS1 is an important target for treating flaviviral infections, and hence, several antibodies are designed against flaviviruses protein for diagnostic and neutralization purposes.[53,62,63] Though several monoclonal antibodies (mAbs) were generated, their targets and structural basis was unknown until the structure of full-length NS1 was solved along with the cross-reactive antibody 2B7.[64] In general, these antibodies target the C-terminal domain and intertwined loop;[65−67] and particularly, the 2B7 monoclonal antibody interacts with two sites, residues 260−316 and 288−344. At the same time, the mutation of residues T301R, A303W, G305 K, E326 K, and D327 K resulted in weaker binding and failed to mediate endothelial hyperpermeability. The mAbs (1Fll, 2E3, 1B2, and 4D2) are specifically reactive to DENV NS1 and 2E11 with other flaviviruses (cross-reactive). The epitope sites recognized by these antibodies are in the intertwined loop (109−123).[67] There are no previous reports on the C-terminal domain interacting with the membrane, and our study shows that the antibody binding sites overlap with the membrane interacting sites. The NS1 C-terminal domain residues E/K272, E/F279, C/C280, P/D281, G/G282, E/E274, E/D278, G/G305, R/K306, R/R324, A/G325, R/E326, G/G328 (ZIKV/DENV residues), and intertwined loop residues 117−123 form stable interactions with the membrane. Our results support the role of the C-terminal domain in cell−surface interaction for inducing endothelial hyperpermeability (as the C-terminal domain is implicated in the membrane binding process). Due to overlapping sites, the mAbs interaction will prevent the NS1 membrane complex formation, which is necessary for viral replication and immune evasion. The difference observed in the interactions of ZIKV and DENV NS1 homologues with the membrane bilayers can also be exploited in designing novel antibodies that can discriminate between ZIKV and DENV infections. Apart from antibodies, small molecules are also developed to inhibit the function of NS1. These small molecules interact with the cavity formed between β-roll, subconnector, and C-terminal domain residues (S/V5, D/S7, F/W8, S/K9, R/K14, C/G16,V/I19, F/F20, I/I21, Y/T22, N/D23, V/V25, E/R192, A/V194, W/W201, R/K214, L/F217).[38,68] Most of the small molecule interacting sites also overlap with the membrane binding residues and hence, the interaction of small molecules would also prevent the membrane affinity of NS1.

Apart from modulating the ER lumen to form the replication complex, NS1 associates with HDL for triggering proinflammatory responses.[29,30,69] Yet, the biologically relevant structure of NS1 in complex with HDL is still questionable. Recently, two cryoEM studies have revealed that the NS1 dimers are anchored to the surface of the HDL particle.[29,32] Interestingly, NS1 dimers are embedded in the HDL through their hydrophobic surface and one end of β-ladder domain is available for antibody binding/interaction. Such an asymmetrical interaction mode is speculated to arise due to the interaction of NS1 with either a lipid or APOAl protein. A similar asymmetrical interaction mode was observed in our study, where only one C-terminal domain interacts with the membrane. Also, both ZIKV and DENV interact well with the cholesterol containing bilayers while ZIKV NS1 shows higher affinity. Altogether, the atomic-level interactions identified in our study highlights the importance of NS1 interaction with the membrane and provide insights to understand the interaction and localization of NS1 with HDL.

We have investigated the NS1 protein's membrane-binding properties using a homogeneous POPE bilayer. We should also consider larger membrane patch to the influence of raft formation and membrane-bending phenomenon. Membrane remodeling by NS1 protein can be studied by employing coarse grain models. These studies are currently in progress in our laboratory.

CONCLUSION

Though the structural folds of ZIKV and DENV NS1 homologues are the same, their corresponding sequences exhibit ∼50% sequence identity. Our findings reveal that ZIKV and DENV NS1 proteins have different binding preferences for different membrane compositions. Differences in ZIKV and DENV NS1 sequences give rise to variation in their electrostatic potential, which further influences their binding to the membrane. This could be due to the differences in the ZIKV and DENV NS1 sequences. As seen from the results, electrostatic interactions along with the hydrophobic interactions promote NS1 binding with the membrane. The stronger membrane-binding property of ZIKV NS1 could be due to the higher basic nature of its inner face than its counterpart in DENV. The contribution of electrostatic interactions for NS1 binding to the membrane is more pronounced in ZIKV than in DENV. Along with positively charged residues, they drive the membrane interactions supporting the experimental study.[70] We have identified key residues necessary for maintaining the NS1-membrane complex from atomic-level interaction analysis, and these findings are consistent with earlier mutational studies. The greater interaction of ZIKV may be responsible for its enhanced remodeling ability reported in the experimental study.[25] These interacting residues also match the predicted epitope locations on NS1,[71,72] particularly the intertwined loop regions (residues 108−129), the α/β subdomain of wing domain (residues 70−84), the C-terminal domain regions (residues 257−274), and the peptide inhibitor binding sites on the β-roll and C-terminal domain. Despite the fact that the domains of ZIKV and DENV NS1 interacting with the membrane are structurally similar, the nature of their stabilizing contacts differs due to the differences in the residues present in these domains. As a result, the strength of binding with membranes of various compositions also changes. We speculate that variations observed in binding with lipid membranes are likely to allosterically modulate the viral replication process and in turn influence other properties. The findings have implications for the development of novel antibodies and possible drugs which will disrupt these interactions and design flaviviral specific treatment methods.

ASSOCIATED CONTENT

Data Availability Statement

In this study, we have used the experimentally determined crystal structures of NS1 proteins from Zika and Dengue viruses with PDB codes 5K6K and 4O6B. These structures can be downloaded from the Protein Data Bank (https://www.rcsb.org/). Molecular dynamics simulations were carried out using GROMACS ver 5.1 (https://www.gromacs.org/). The minimized coordinates of each system, index files, topology and molecular dynamics.mdp files are available in the GitHub repository (https://github.com/ramasubbu-sankar/zika-virus-NS1-MD). The data (MD trajectories) obtained in this work

https://doi.org/10.1021/acsbiomedchemau.3c00073
ACS Bio Med Chem Au 2024, 4, 137−153

and the in-house scripts can be obtained from the authors of the manuscript upon reasonable request.

Supporting Information

The Supporting Information is available free of charge at https://pubs.acs.org/doi/10.1021/acsbiomedchemau.3c00073.

> Tables for the structural properties of lipid bilayers, interaction energies between NS1 and lipid bilayer; order parameter of lipid bilayers, pairwise sequence alignment between ZIKV and DENV NS1, RMSD of NS1 without intertwined loop, RMSD of individual monomers, RMSF plots of NS1 proteins, MD snapshots of ZIKV and DENV, distance and angle between NS1 and membrane for independent replicates, density profiles of individual domains of NS1 for chain B of ZIKV and DENV, secondary structure analysis of intertwined loop region of ZIKV and DENV NS1, distance between intertwined loop residues and center of mass of membrane, electrostatic potentials of NS1 systems; details of MD simulations of model membrane and bilayers properties (PDF)

AUTHOR INFORMATION

Corresponding Authors

Ramasubbu Sankararamakrishnan − *Department of Biological Sciences and Bioengineering and Mehta Family Center for Engineering in Medicine, Indian Institute of Technology Kanpur, Kanpur 208016, India;* orcid.org/0000-0002-8527-5614; Email: rsankar@iitk.ac.in

Rajagopalan Muthukumaran − *Department of Biological Sciences and Bioengineering, Indian Institute of Technology Kanpur, Kanpur 208016, India*; Phone: +91 512 259 4014; Email: kumaranbioinfo@gmail.com; Fax: +91 512 2594010

Complete contact information is available at: https://pubs.acs.org/10.1021/acsbiomedchemau.3c00073

Author Contributions

CRediT: **Rajagopalan Muthukumaran** conceptualization, data curation, formal analysis, investigation, writing-original draft, writing-review & editing; **Ramasubbu Sankararamakrishnan** conceptualization, data curation, formal analysis, funding acquisition, methodology, project administration, resources, supervision, writing-original draft, writing-review & editing.

Notes

The authors declare no competing financial interest.

ACKNOWLEDGMENTS

M.R. would like to acknowledge DBT-RA program in Biotechnology and Life Sciences for Research Associate fellowship and Institute Postdoctoral fellowship from IIT-Kanpur. R.S. was Pradeep Sindhu Chair Professor at the time of this investigation. We thank the High-performance computing and Param Sanganak facility at IIT-Kanpur for the computational resources. We thank all our lab members for useful discussion. We gratefully acknowledge IIT-Kanpur for financial assistance.

REFERENCES

(1) Bhatt, S.; Gething, P. W.; Brady, O. J.; Messina, J. P.; Farlow, A. W.; Moyes, C. L.; Drake, J. M.; Brownstein, J. S.; Hoen, A. G.; Sankoh, O.; Myers, M. F.; George, D. B.; Jaenisch, T.; Wint, G. R.; Simmons, C. P.; Scott, T. W.; Farrar, J. J.; Hay, S. I. The global distribution and burden of dengue. *Nature* **2013**, *496* (7446), 504−7.

(2) Pierson, T. C.; Diamond, M. S. The emergence of Zika virus and its new clinical syndromes. *Nature* **2018**, *560* (7720), 573−581.

(3) Roehrig, J. T. West nile virus in the United States - a historical perspective. *Viruses* **2013**, *5* (12), 3088−108.

(4) Pierson, T. C.; Diamond, M. S. The continued threat of emerging flaviviruses. *Nat. Microbiol* **2020**, *5* (6), 796−812.

(5) Sanchez-Montalva, A.; Salvador, F.; Molina, I. Persistence of Zika Virus in Body Fluids - Final Report. *N Engl J. Med.* **2019**, *380* (2), 198.

(6) Mead, P. S.; Duggal, N. K.; Hook, S. A.; Delorey, M.; Fischer, M.; Olzenak McGuire, D.; Becksted, H.; Max, R. J.; Anishchenko, M.; Schwartz, A. M.; Tzeng, W. P.; Nelson, C. A.; McDonald, E. M.; Brooks, J. T.; Brault, A. C.; Hinckley, A. F. Zika Virus Shedding in Semen of Symptomatic Infected Men. *N Engl J. Med.* **2018**, *378* (15), 1377−1385.

(7) Gubler, D. J. Dengue/dengue haemorrhagic fever: history and current status. *Novartis Found Symp.* **2006**, *277*, 3−16 discussion 16−22, 71−3, 251−3.

(8) Yun, S. I.; Lee, Y. M. Zika virus: An emerging flavivirus. *J. Microbiol* **2017**, *55* (3), 204−219.

(9) Tabata, T.; Petitt, M.; Puerta-Guardo, H.; Michlmayr, D.; Wang, C.; Fang-Hoover, J.; Harris, E.; Pereira, L. Zika Virus Targets Different Primary Human Placental Cells, Suggesting Two Routes for Vertical Transmission. *Cell Host Microbe* **2016**, *20* (2), 155−66.

(10) Gupta, N.; Kodan, P.; Baruah, K.; Soneja, M.; Biswas, A. Zika virus in India: past, present and future. *QJM* **2023**, *116*, 644−649.

(11) Petersen, E.; Wilson, M. E.; Touch, S.; McCloskey, B.; Mwaba, P.; Bates, M.; Dar, O.; Mattes, F.; Kidd, M.; Ippolito, G.; Azhar, E. I.; Zumla, A. Rapid Spread of Zika Virus in The Americas-Implications for Public Health Preparedness for Mass Gatherings at the 2016 Brazil Olympic Games. *Int. J. Infect Dis* **2016**, *44*, 11−5.

(12) Rolph, M. S.; Mahalingam, S. Zika's passage to India. *Lancet Infect Dis* **2019**, *19* (5), 469−470.

(13) Musso, D.; Gubler, D. J. Zika Virus. *Clin Microbiol Rev.* **2016**, *29* (3), 487−524.

(14) Watterson, D.; Modhiran, N.; Young, P. R. The many faces of the flavivirus NS1 protein offer a multitude of options for inhibitor design. *Antiviral Res.* **2016**, *130*, 7−18.

(15) Rastogi, M.; Sharma, N.; Singh, S. K. Flavivirus NS1: a multifaceted enigmatic viral protein. *Virol J.* **2016**, *13*, 131.

(16) Gutsche, I.; Coulibaly, F.; Voss, J. E.; Salmon, J.; d'Alayer, J.; Ermonval, M.; Larquet, E.; Charneau, P.; Krey, T.; Megret, F.; Guittet, E.; Rey, F. A.; Flamand, M. Secreted dengue virus nonstructural protein NS1 is an atypical barrel-shaped high-density lipoprotein. *Proc. Natl. Acad. Sci. U. S. A.* **2011**, *108* (19), 8003−8.

(17) Lindenbach, B. D.; Rice, C. M. Molecular biology of flaviviruses. *Adv. Virus Res.* **2003**, *59*, 23−61.

(18) Lo, N. T. N.; Roodsari, S. Z.; Tin, N. L.; Wong, M. P.; Biering, S. B.; Harris, E. Molecular Determinants of Tissue Specificity of Flavivirus Nonstructural Protein 1 Interaction with Endothelial Cells. *J. Virol* **2022**, *96* (19), No. e0066122.

(19) Shi, Y.; Gao, G. F. Structural Biology of the Zika Virus. *Trends Biochem. Sci.* **2017**, *42* (6), 443−456.

(20) Glasner, D. R.; Puerta-Guardo, H.; Beatty, P. R.; Harris, E. The Good, the Bad, and the Shocking: The Multiple Roles of Dengue Virus Nonstructural Protein 1 in Protection and Pathogenesis. *Annu. Rev. Virol* **2018**, *5* (1), 227−253.

(21) Akey, D. L.; Brown, W. C.; Dutta, S.; Konwerski, J.; Jose, J.; Jurkiw, T. J.; DelProposto, J.; Ogata, C. M.; Skiniotis, G.; Kuhn, R. J.; Smith, J. L. Flavivirus NS1 structures reveal surfaces for associations with membranes and the immune system. *Science* **2014**, *343* (6173), 881−5.

(22) Brown, W. C.; Akey, D. L.; Konwerski, J. R.; Tarrasch, J. T.; Skiniotis, G.; Kuhn, R. J.; Smith, J. L. Extended surface for membrane

association in Zika virus NS1 structure. *Nat. Struct Mol. Biol.* **2016**, *23* (9), 865−7.
(23) Xu, X.; Song, H.; Qi, J.; Liu, Y.; Wang, H.; Su, C.; Shi, Y.; Gao, G. F. Contribution of intertwined loop to membrane association revealed by Zika virus full-length NS1 structure. *EMBO J.* **2016**, *35* (20), 2170−2178.
(24) Akey, D. L.; Brown, W. C.; Jose, J.; Kuhn, R. J.; Smith, J. L. Structure-guided insights on the role of NS1 in flavivirus infection. *Bioessays* **2015**, *37* (5), 489−94.
(25) Ci, Y.; Liu, Z. Y.; Zhang, N. N.; Niu, Y.; Yang, Y.; Xu, C.; Yang, W.; Qin, C. F.; Shi, L. Zika NS1-induced ER remodeling is essential for viral replication. *J. Cell Biol.* **2020**, *219* (2), e201903062.
(26) Noisakran, S.; Dechtawewat, T.; Avirutnan, P.; Kinoshita, T.; Siripanyaphinyo, U.; Puttikhunt, C.; Kasinrerk, W.; Malasit, P.; Sittisombut, N. Association of dengue virus NS1 protein with lipid rafts. *J. Gen Virol* **2008**, *89* (10), 2492−2500.
(27) Soto-Acosta, R.; Mosso, C.; Cervantes-Salazar, M.; Puerta-Guardo, H.; Medina, F.; Favari, L.; Ludert, J. E.; del Angel, R. M. The increase in cholesterol levels at early stages after dengue virus infection correlates with an augment in LDL particle uptake and HMG-CoA reductase activity. *Virology* **2013**, *442* (2), 132−47.
(28) Chen, Q.; Gouilly, J.; Ferrat, Y. J.; Espino, A.; Glaziou, Q.; Cartron, G.; El Costa, H.; Al-Daccak, R.; Jabrane-Ferrat, N. Metabolic reprogramming by Zika virus provokes inflammation in human placenta. *Nat. Commun.* **2020**, *11* (1), 2967.
(29) Benfrid, S.; Park, K. H.; Dellarole, M.; Voss, J. E.; Tamietti, C.; Pehau-Arnaudet, G.; Raynal, B.; Brule, S.; England, P.; Zhang, X.; Mikhailova, A.; Hasan, M.; Ungeheuer, M. N.; Petres, S.; Biering, S. B.; Harris, E.; Sakuntabhai, A.; Buchy, P.; Duong, V.; Dussart, P.; Coulibaly, F.; Bontems, F.; Rey, F. A.; Flamand, M. Dengue virus NS1 protein conveys pro-inflammatory signals by docking onto high-density lipoproteins. *EMBO Rep* **2022**, *23* (7), No. e53600.
(30) Alcala, A. C.; Ludert, J. E. The dengue virus NS1 protein; new roles in pathogenesis due to similarities with and affinity for the high-density lipoprotein (HDL)? *PLoS Pathog* **2023**, *19* (8), No. e1011587.
(31) Modhiran, N.; Watterson, D.; Muller, D. A.; Panetta, A. K.; Sester, D. P.; Liu, L.; Hume, D. A.; Stacey, K. J.; Young, P. R. Dengue virus NS1 protein activates cells via Toll-like receptor 4 and disrupts endothelial cell monolayer integrity. *Sci. Transl Med.* **2015**, *7* (304), 304ra142.
(32) Chew, B. L. A.; Ngoh, A. Q.; Phoo, W. W.; Chan, K. W. K.; Ser, Z.; Tulsian, N. K.; Lim, S. S.; Weng, M. J. G.; Watanabe, S.; Choy, M. M.; Low, J. G.; Ooi, E. E.; Ruedl, C.; Sobota, R. M.; Vasudevan, S. G.; Luo, D. Secreted dengue virus NS1 from infection is predominantly dimeric and in complex with high-density lipoprotein. *BioRxiv*, November 21, 2023, ver. 1. (accessed 2024-02-29).
(33) Hilgenfeld, R. Zika virus NS1, a pathogenicity factor with many faces. *EMBO J.* **2016**, *35* (24), 2631−2633.
(34) Poveda-Cuevas, S. A.; Etchebest, C.; Barroso da Silva, F. L. Insights into the ZIKV NS1 Virology from Different Strains through a Fine Analysis of Physicochemical Properties. *ACS Omega* **2018**, *3* (11), 16212−16229.
(35) Muller, D. A.; Young, P. R. The flavivirus NS1 protein: molecular and structural biology, immunology, role in pathogenesis and application as a diagnostic biomarker. *Antiviral Res.* **2013**, *98* (2), 192−208.
(36) Oliveira, E. R.; de Alencastro, R. B.; Horta, B. A. The mechanism by which P250L mutation impairs flavivirus-NS1 dimerization: an investigation based on molecular dynamics simulations. *Eur. Biophys J.* **2016**, *45* (6), 573−80.
(37) Roy, P.; Roy, S.; Sengupta, N. Disulfide Reduction Allosterically Destabilizes the beta-Ladder Subdomain Assembly within the NS1 Dimer of ZIKV. *Biophys. J.* **2020**, *119* (8), 1525−1537.
(38) Raza, S.; Abbas, G.; Azam, S. S. Screening Pipeline for Flavivirus Based Inhibitors for Zika Virus NS1. *IEEE/ACM Trans Comput. Biol. Bioinform* **2020**, *17* (5), 1751−1761.
(39) Songprakhon, P.; Thaingtamtanha, T.; Limjindaporn, T.; Puttikhunt, C.; Srisawat, C.; Luangaram, P.; Dechtawewat, T.; Uthaipibull, C.; Thongsima, S.; Yenchitsomanus, P. T.; Malasit, P.; Noisakran, S. Peptides targeting dengue viral nonstructural protein 1 inhibit dengue virus production. *Sci. Rep* **2020**, *10* (1), 12933.
(40) Pessoa, R.; Patriota, J. V.; Lourdes de Souza, M.; Felix, A. C.; Mamede, N.; Sanabani, S. S. Investigation Into an Outbreak of Dengue-like Illness in Pernambuco, Brazil, Revealed a Cocirculation of Zika, Chikungunya, and Dengue Virus Type 1. *Medicine (Baltimore)* **2016**, *95* (12), No. e3201.
(41) Lanciotti, R. S.; Kosoy, O. L.; Laven, J. J.; Velez, J. O.; Lambert, A. J.; Johnson, A. J.; Stanfield, S. M.; Duffy, M. R. Genetic and serologic properties of Zika virus associated with an epidemic, Yap State, Micronesia, 2007. *Emerg Infect Dis* **2008**, *14* (8), 1232−9.
(42) Lee, A. J.; Bhattacharya, R.; Scheuermann, R. H.; Pickett, B. E. Identification of diagnostic peptide regions that distinguish Zika virus from related mosquito-borne Flaviviruses. *PLoS One* **2017**, *12* (5), No. e0178199.
(43) Mishra, N.; Caciula, A.; Price, A.; Thakkar, R.; Ng, J.; Chauhan, L. V.; Jain, K.; Che, X.; Espinosa, D. A.; Montoya Cruz, M.; Balmaseda, A.; Sullivan, E. H.; Patel, J. J.; Jarman, R. G.; Rakeman, J. L.; Egan, C. T.; Reusken, C.; Koopmans, M. P. G.; Harris, E.; Tokarz, R.; Briese, T.; Lipkin, W. I. Diagnosis of Zika Virus Infection by Peptide Array and Enzyme-Linked Immunosorbent Assay. *mBio* **2018**, *9* (2), e00095-18.
(44) Amrun, S. N.; Yee, W. X.; Abu Bakar, F.; Lee, B.; Kam, Y. W.; Lum, F. M.; Tan, J. J.; Lim, V. W.; Watthanaworawit, W.; Ling, C.; Nosten, F.; Renia, L.; Leo, Y. S.; Ng, L. F. Novel differential linear B-cell epitopes to identify Zika and dengue virus infections in patients. *Clin Transl Immunology* **2019**, *8* (7), No. e1066.
(45) Abraham, M. J.; Murtola, T.; Schulz, R.; Páll, S.; Smith, J. C.; Hess, B.; Lindahl, E. GROMACS: High performance molecular simulations through multi-level parallelism from laptops to supercomputers. *SoftwareX* **2015**, *1−2*, 19−25.
(46) Jorgensen, W. L.; Chandrasekhar, J.; Madura, J. D.; Impey, R. W.; Klein, M. L. Comparison of simple potential functions for simulating liquid water. *J. Chem. Phys.* **1983**, *79* (2), 926−935.
(47) Bussi, G.; Donadio, D.; Parrinello, M. Canonical sampling through velocity rescaling. *J. Chem. Phys.* **2007**, *126* (1), 014101.
(48) Parrinello, M.; Rahman, A. Polymorphic transitions in single crystals: A new molecular dynamics method. *J. Appl. Phys.* **1981**, *52* (12), 7182−7190.
(49) Darden, T.; York, D.; Pedersen, L. Particle mesh Ewald: An N·log(N) method for Ewald sums in large systems. *J. Chem. Phys.* **1993**, *98* (12), 10089−10092.
(50) Baker, N. A.; Sept, D.; Joseph, S.; Holst, M. J.; McCammon, J. A. Electrostatics of nanosystems: application to microtubules and the ribosome. *Proc. Natl. Acad. Sci. U. S. A.* **2001**, *98* (18), 10037−41.
(51) Jurrus, E.; Engel, D.; Star, K.; Monson, K.; Brandi, J.; Felberg, L. E.; Brookes, D. H.; Wilson, L.; Chen, J.; Liles, K.; Chun, M.; Li, P.; Gohara, D. W.; Dolinsky, T.; Konecny, R.; Koes, D. R.; Nielsen, J. E.; Head-Gordon, T.; Geng, W.; Krasny, R.; Wei, G. W.; Holst, M. J.; McCammon, J. A.; Baker, N. A. Improvements to the APBS biomolecular solvation software suite. *Protein Sci.* **2018**, *27* (1), 112−128.
(52) Pettersen, E. F.; Goddard, T. D.; Huang, C. C.; Couch, G. S.; Greenblatt, D. M.; Meng, E. C.; Ferrin, T. E. UCSF Chimera-a visualization system for exploratory research and analysis. *J. Comput. Chem.* **2004**, *25* (13), 1605−12.
(53) Edeling, M. A.; Diamond, M. S.; Fremont, D. H. Structural basis of Flavivirus NS1 assembly and antibody recognition. *Proc. Natl. Acad. Sci. U. S. A.* **2014**, *111* (11), 4285−90.
(54) Goncalves, R. L.; de Lima Menezes, G.; Sussuchi, L.; Moreli, M. L.; Mottin, M.; Andrade, C. H.; Pereira, M.; da Silva, R. A. Dynamic behavior of Dengue and Zika viruses NS1 protein reveals monomer-monomer interaction mechanisms and insights to rational drug design. *J. Biomol Struct Dyn* **2020**, *38* (14), 4353−4363.
(55) Kapuganti, S. K.; Kumar, P.; Giri, R. Structural dynamics of Zika virus NS1 via a reductionist approach reveal the disordered nature of its beta-roll domain in isolation. *Virology* **2022**, *573*, 72−83.
(56) Poveda Cuevas, S. A.; Barroso da Silva, F. L.; Etchebest, C. NS1 from Two Zika Virus Strains Differently Interact with a Membrane:

Insights to Understand Their Differential Virulence. *J. Chem. Inf Model* **2023**, *63* (4), 1386−1400.
(57) Poveda-Cuevas, S. A.; Barroso da Silva, F. L.; Etchebest, C. How the Strain Origin of Zika Virus NS1 Protein Impacts Its Dynamics and Implications to Their Differential Virulence. *J. Chem. Inf Model* **2021**, *61* (3), 1516−1530.
(58) Killian, J. A.; von Heijne, G. How proteins adapt to a membrane-water interface. *Trends Biochem. Sci.* **2000**, *25* (9), 429−434.
(59) Sankararamakrishnan, R.; Weinstein, H. Molecular Dynamics Simulations Predict a Tilted Orientation for the Helical Region of Dynorphin A(1−17) in Dimyristoylphosphatidylcholine Bilayers. *Biophys. J.* **2000**, *79* (5), 2331−2344.
(60) Priyanka, P.; Sankararamakrishnan, R. Molecular Dynamics Simulations of C-Terminal Decapeptide of Gastrin-Releasing Peptide in DMPC Bilayers: Structure, Stability and Orientation of the Peptide Hormone Within the Bilayers. *Protein and Peptide Letters* **2007**, *14* (6), 590−596.
(61) Ulmschneider, M. B.; Sansom, M. S. P. Amino acid distributions in integral membrane protein structures. *Biochimica et Biophysica Acta (BBA) - Biomembranes* **2001**, *1512* (1), 1−14.
(62) Sootichote, R.; Puangmanee, W.; Benjathummarak, S.; Kowaboot, S.; Yamanaka, A.; Boonnak, K.; Ampawong, S.; Chatchen, S.; Ramasoota, P.; Pitaksajjakul, P. Potential Protective Effect of Dengue NS1 Human Monoclonal Antibodies against Dengue and Zika Virus Infections. *Biomedicines* **2023**, *11* (1), 227.
(63) Wessel, A. W.; Kose, N.; Bombardi, R. G.; Roy, V.; Chantima, W.; Mongkolsapaya, J.; Edeling, M. A.; Nelson, C. A.; Bosch, I.; Alter, G.; Screaton, G. R.; Fremont, D. H.; Crowe, J. E., Jr; Diamond, M. S. Antibodies targeting epitopes on the cell-surface form of NS1 protect against Zika virus infection during pregnancy. *Nat. Commun.* **2020**, *11* (1), 5278.
(64) Biering, S. B.; Akey, D. L.; Wong, M. P.; Brown, W. C.; Lo, N. T. N.; Puerta-Guardo, H.; Tramontini Gomes de Sousa, F.; Wang, C.; Konwerski, J. R.; Espinosa, D. A.; Bockhaus, N. J.; Glasner, D. R.; Li, J.; Blanc, S. F.; Juan, E. Y.; Elledge, S. J.; Mina, M. J.; Beatty, P. R.; Smith, J. L.; Harris, E. Structural basis for antibody inhibition of flavivirus NS1-triggered endothelial dysfunction. *Science* **2021**, *371* (6525), 194−200.
(65) Hertz, T.; Beatty, P. R.; MacMillen, Z.; Killingbeck, S. S.; Wang, C.; Harris, E. Antibody Epitopes Identified in Critical Regions of Dengue Virus Nonstructural 1 Protein in Mouse Vaccination and Natural Human Infections. *J. Immunol* **2017**, *198* (10), 4025−4035.
(66) Lai, Y. C.; Chuang, Y. C.; Liu, C. C.; Ho, T. S.; Lin, Y. S.; Anderson, R.; Yeh, T. M. Antibodies Against Modified NS1 Wing Domain Peptide Protect Against Dengue Virus Infection. *Sci. Rep* **2017**, *7* (1), 6975.
(67) Luangaram, P.; Tamdet, C.; Saengwong, C.; Prommool, T.; Kraivong, R.; Nilchan, N.; Punyadee, N.; Avirutnan, P.; Srisawat, C.; Malasit, P.; Kasinrerk, W.; Puttikhunt, C. Differential critical residues on the overlapped region of the non-structural protein-1 recognized by flavivirus and dengue virus cross-reactive monoclonal antibodies. *Sci. Rep* **2022**, *12* (1), 21548.
(68) de Lima Menezes, G.; Vogel Saivish, M.; Lacerda Nogueira, M.; Alves da Silva, R. Virtual screening of small natural compounds against NS1 protein of DENV, YFV and ZIKV. *J. Biomol Struct Dyn* **2023**, *41* (7), 2981−2991.
(69) Coelho, D. R.; Carneiro, P. H.; Mendes-Monteiro, L.; Conde, J. N.; Andrade, I.; Cao, T.; Allonso, D.; White-Dibiasio, M.; Kuhn, R. J.; Mohana-Borges, R. ApoA1 Neutralizes Proinflammatory Effects of Dengue Virus NS1 Protein and Modulates Viral Immune Evasion. *J. Virol* **2021**, *95* (13), No. e0197420.
(70) Ci, Y.; Yang, Y.; Xu, C.; Qin, C. F.; Shi, L. Electrostatic Interaction Between NS1 and Negatively Charged Lipids Contributes to Flavivirus Replication Organelles Formation. *Front Microbiol* **2021**, *12*, 641059.
(71) Freire, M.; Pol-Fachin, L.; Coelho, D. F.; Viana, I. F. T.; Magalhaes, T.; Cordeiro, M. T.; Fischer, N.; Loeffler, F. F.; Jaenisch, T.; Franca, R. F.; Marques, E. T. A.; Lins, R. D. Mapping Putative B-Cell Zika Virus NS1 Epitopes Provides Molecular Basis for Anti-NS1 Antibody Discrimination between Zika and Dengue Viruses. *ACS Omega* **2017**, *2* (7), 3913−3920.
(72) Lee, H. J.; Cho, Y.; Kang, H. J.; Choi, H.; Han, K. R.; Chong, C. K.; Kim, Y. B. Identification of peptide based B-cell epitopes in Zika virus NS1. *Biochem. Biophys. Res. Commun.* **2018**, *505* (4), 1010−1014.

https://doi.org/10.1021/acsbiomedchemau.3c00073
ACS Bio Med Chem Au 2024, 4, 137−153